VOLUME 70, NUMBER 10, OCTOBER 2016

EVOLUTION

INTERNATIONAL JOURNAL OF ORGANIC EVOLUTION

Published by the Society
for the Study of Evolution

doi:10.1111/evo.13021

Correlated evolution of body and fin morphology in the cichlid fishes

Kara L. Feilich[1,2]

[1]*Museum of Comparative Zoology, Harvard University, Cambridge, Massachusetts 02138*

[2]*E-mail: kfeilich@fas.harvard.edu*

Received November 21, 2015
Accepted July 19, 2016

Body and fin shapes are chief determinants of swimming performance in fishes. Different configurations of body and fin shapes can suit different locomotor specializations. The success of any configuration is dependent upon the hydrodynamic interactions between body and fins. Despite the importance of body–fin interactions for swimming, there are few data indicating whether body and fin configurations evolve in concert, or whether these structures vary independently. The cichlid fishes are a diverse family whose well-studied phylogenetic relationships make them ideal for the study of macroevolution of ecomorphology. This study measured body, and caudal and median fin morphology from radiographs of 131 cichlid genera, using morphometrics and phylogenetic comparative methods to determine whether these traits exhibit correlated evolution. Partial least squares canonical analysis revealed that body, caudal fin, dorsal fin, and anal fin shapes all exhibited strong correlated evolution consistent with locomotor ecomorphology. Major patterns included the evolution of deep body profiles with long fins, suggestive of maneuvering specialization; and the evolution of narrow, elongate caudal peduncles with concave tails, a combination that characterizes economical cruisers. These results demonstrate that body shape evolution does not occur independently of other traits, but among a suite of other morphological changes that augment locomotor specialization.

KEY WORDS: **Adaptive radiation, anal fin, caudal fin, Cichlidae, correlated evolution, dorsal fin, geometric morphometrics, locomotion.**

The explosive speciation and diversification of cichlid fishes has made the group an ideal model system for the study of evolution and adaptation. In addition to taxonomically diverse clades endemic to the African rift lakes, the family also includes morphologically and behaviorally diverse fishes from South America, West Africa, and the Indian subcontinent (Liem 1973; Genner et al. 2007). In the context of extensive and robust phylogenetic hypotheses of cichlid interrelationships (Salzburger et al. 2005; Genner et al. 2007; Friedman et al. 2013; McMahan et al. 2013; Schwarzer et al. 2015, and others), comparative biologists focusing on this lineage are afforded the opportunity to study the process and mechanisms that underpin adaptive radiation, and the evolution of morphological systems that are implicated in the group's adaptive success. Several studies have focused on the explosive cichlid radiation to study the process of morphological evolution (Liem 1973; Kocher et al. 1993; Winemiller et al. 1995; Albertson et al. 2003; Clabaut et al. 2007; Young et al. 2009), with some recent studies exploring the evolution of functionally related structures (Rüber and Adams 2001; Muschick et al. 2012; Kusche et al. 2014; Astudillo-Clavijo et al. 2015).

Although many morphological studies focus on body shape in isolation, there is a large body of work showing that fin morphology may be just as important as body shape. Fin shape and configuration vary widely, and serve multiple functions during swimming, including thrust production, stabilization, and maneuvering (Webb 1982, 1984; Weihs 1989; Lauder et al. 2002; Lauder and Drucker 2004). The role of pectoral fin shape and kinematics in swimming performance has been discussed for several labriform taxa (Walker and Westneat 2002; Thorsen and Westneat 2005), and median fin variation has been discussed with respect to balistiform locomotion (Wright 2000; Blake et al. 2009; Dornberg et al. 2011). Biomechanists have long considered caudal fin shape in its relation to swimming performance, particularly in the context of swimming economy (e.g., Affleck 1950; Borazjani

EVOLUTION
INTERNATIONAL JOURNAL OF ORGANIC EVOLUTION

and Daghoogi 2013). Species descriptions and the taxonomic literature refer often to meristic counts of fin elements in the median fins, but rarely consider the shapes of fins in explicitly functional contexts. In one study, Dornberg et al. (2011) examined the correlations between fin and body shapes within triggerfishes (family Balistidae). However, given the unique mode of locomotion in this group—"balistiform" swimming, in which dorsal and anal fins are the main propulsors—it is unlikely that the patterns they uncovered apply generally to nonbalistid fishes. The functional roles of different fin shapes have been considered in several earlier studies including those using physical (Affleck 1950; Lauder et al. 2012; Feilich and Lauder 2015), theoretical (Lighthill 1970), and computational models (Borazjani and Daghoogi 2013).

To exclude midline fins from the morphometrics literature belies their importance for locomotion. In some fishes, such as bluegill (*Lepomis macrochirus*), the dorsal fin alone may account for more than 10% of total thrust production during steady swimming, and over a third of the lateral forces during turning (Drucker and Lauder 2001). Caudal peduncle and caudal fin morphology have been discussed in the biomechanics literature as having the potential to reduce drag, increase thrust, and interact with the median fins during locomotion, but this has not been explored in an explicitly phylogenetic context (Weihs 1989; Triantafyllou et al. 2000). Recent biomechanics research provides increasing evidence that fin–fin and fin–body interactions may be very important in terms of their ability to explain the effect of potential morphological adaptations on locomotor performance (Akhtar et al. 2007; Tytell et al. 2008; Feilich and Lauder 2015).

Given the importance of the fins and body operating in tandem to facilitate swimming and feeding, the question arises as to whether fin and body shape evolution are tightly correlated, or whether body and fins largely evolve independently of one another. This study leverages the diversity of cichlid body and fin morphology and the strong history of cichlid evolutionary morphology to investigate how fins and body shape covary and evolve within the lineage. To answer this question, I take a comparative morphometric approach, examining the variety of cichlid shapes, and any patterns of correlated evolution among fins and body.

Previous studies of cichlid body shape evolution have demonstrated consistent patterns in variation among several cichlid clades. The major axis of cichlid body–shape diversity, as in many other fishes, appears to be body elongation (Clabaut et al. 2007; Friedman 2010; Muschick et al. 2012; Claverie and Wainwright 2014; Astudillo-Clavijo et al. 2015). Elongation is largely associated with increases in vertebral count, vertebral length, and/or with elongation of the "snout" (Ward and Mehta 2010). Most cichlid morphospaces, and many morphospaces for other fish taxa, also suggest that variation in isolated regions of the body (e.g., caudal peduncle depth and length, head length) contribute significantly to overall morphological disparity (Clabaut et al. 2007; Claverie and Wainwright 2014; Montaña et al. 2014).

Studies of both feeding morphology and body shape, among cichlids and ecologically similar species, provide strong evidence of an ecomorphological link between both body shape and pharyngeal jaw morphology with trophic niche (Winemiller et al. 1995; Rüber and Adams 2001; Clabaut et al. 2007; Muschick et al. 2012; López-Fernández et al. 2012). For example, piscivores tend to have long shallow heads, and large anterior bodies (Clabaut et al. 2007; López-Fernández et al. 2012). This pattern in trophic ecomorphology has also been described in other fishes, including temperate sunfishes (Ehlinger and Wilson 1988), arctic char (Snorrason et al. 1994), and sea breams (Antonucci et al. 2009).

Within cichlids, some clades exhibit more body shape variation than others. Studies of all African cichlids show that while the species richness of the haplochromine radiation is astounding, within-group morphological variation of the haplochromines is lower than that of the paraphyletic Tanganyikan and West African nonhaplochromine cichlids (Chakrabarty 2005). In the neotropical cichlids, the geophagines have the highest within group body shape variation (Arbour and López-Fernández 2014). To date, no studies have compared the morphological variation across both African and Neotropical cichlid clades.

This study makes use of the vast morphological diversity of cichlids and builds on earlier morphometric studies of fish evolution to fill the gap in the literature as to body and median fin covariation. I measured body and fin morphology in 131 cichlid genera, and used two separate phylogenetic hypotheses of cichlid evolution to assess the extent to which morphological evolution of individual structures and correlated evolution among structures occurred. I hypothesized that if body and fin shape were constrained according to existing hypotheses of locomotor specialization, extremes in body and fin shape would co-occur in patterns consistent with those hypotheses (Table 1). Specifically, a set of predictions were made derived from the oft-applied (though less-oft-tested) hypotheses proposed by Webb (1984), with two different null predictions, explained in Table 1.

Null hypothesis 1 is the prediction expected given complete modularity of body and fins, with changes in one structure occurring independently of changes in any other structure, with low integration across structures. Null hypothesis 2 is the opposite prediction, that all structures exhibit perfect covariation and correlated evolution, with high integration across all structures. These null hypotheses were unlikely to explain cichlid morphology, but provided a basis for comparison to check for other patterns in morphological evolution. The alternative hypotheses describe patterns of correlated evolution that one may expect given selection for locomotion-related configurations. These hypotheses predict patterns of linkage between structures that interact during

Table 1. Framework and rationale for hypotheses describing evolutionary covariation.

	Hypothesis	Prediction	Rationale
Null hypotheses	Null 1: Complete modularity	No morphological covariation between any structure pairing.	In a rapidly evolving clade, it is possible that all structures are effectively evolving independently and/or that there is no selection for correlated evolution of structures.
	Null 2: Complete covariation	All structures exhibit perfectly correlated evolution, with similar patterns of disparity through time.	If the body and fins are actually a single unit, and the distinction among them is merely a useful tool for descriptive anatomy, and/or if selection for correlated evolution is very strong (i.e., only very few combinations of traits satisfy the organism's functional needs), then one would expect all structures to evolve together.
Functional linkage hypotheses	Link 1: Body–caudal fin	Body shape and caudal fin shape exhibit correlated evolution, with similar patterns of disparity through time.	Species specializing in steady swimming economy are expected to have both a fusiform "tuna-like" shape, and forked or semi-lunate tails to reduce drag and increase thrust during body–caudal fin swimming (Lighthill 1970, Webb 1984, Weihs 1989, Feilich and Lauder 2015). Therefore, if swimming economy is a major selective pressure on morphology, one may expect to see correlated evolution of these two propulsive structures.
	Link 2: Dorsal fin–anal fin	Dorsal fin shape and anal fin shape exhibit correlated evolution, with similar patterns of disparity through time.	There are both functional and developmental linkages between the dorsal and anal fin. The dorsal and anal fin form symmetrically about the longitudinal axis of the fish, suggesting that they are a developmental module (Mabee et al. 2002). Their function in stabilizing roll and maneuver may be enhanced by symmetric structure as well.
	Link 3: Body–caudal fin Body–dorsal fin Caudal fin–dorsal fin	Body, caudal fin, and dorsal fin will all exhibit correlated evolution with similar patterns of disparity through time.	See body–caudal fin module hypothesis, and the dorsal fin may play a role in wake recapture and drag reduction by interacting with flow shed by the body and orienting it relative to the leading edge of the tail to increase thrust (Tytell et al. 2008, Borazjani and Daghoogi 2013, Feilich and Lauder 2015).
	Link 4: Body–dorsal fin Body–anal fin Dorsal fin–anal fin	Body, dorsal fin, and anal fin will all exhibit correlated evolution with similar patterns of disparity through time.	See dorsal fin–anal fin module, and a deep-bodied, round lateral profile are thought to permit greater turning moments in maneuvering specialists (Webb 1984).

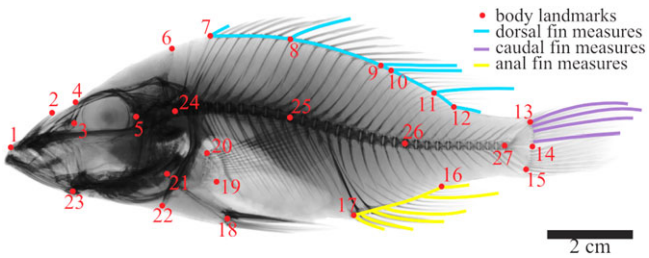

Figure 1. Body landmarks and fin lengths used in morphometric analyses, shown on a representative specimen (MCZ 49441 *Stigmatochromis woodi*). To analyze shape independently of size, generalized Procrustes coordinates were used to compare body shape, fin base lengths were expressed as the ratio of fin base length to total length, and fin element lengths were expressed as the residual of fin element length on centroid size.

undulatory swimming, described in Table 1. Correlated evolution between the structures in the alternative hypotheses would reflect evolution toward an expected locomotor specialist phenotype.

Methods

MORPHOLOGICAL DATA COLLECTION

Morphological diversity in cichlids is generally believed to be highest at the intergeneric level, with only minor differences in morphology within genera (Stauffer et al. 1997; Albertson et al. 1999; López-Fernández et al. 2012); so sampling efforts focused on measuring as many different genera as possible. One hundred and thirty-one cichlid museum specimens were obtained from the MCZ or AMNH (Table S1), and a specimen radiograph of *Retroculus* was obtained from the NMNH Ichthyology collection database. All specimens were adults in good condition, and if any structure was damaged, it was excluded from the analysis of that structure. It was assumed that differences in morphology due to initial method of preservation (formalin or ethanol fixation) or specimen age would be minimal compared to variation from differences in species morphology (Lai 1963). For those species known to exhibit sexual dimorphism, specimens that were either female or indistinguishable from female were used. Specimens were imaged using a Kevex PXS10-16W x-ray source (Thermo Electron Corp., Scotts Valley, CA), and a PaxScan 4030R digital imaging subsystem (Varian Medical Systems, Salt Lake City, UT). These radiographs were used to obtain data for subsequent analysis.

Twenty-seven geometric morphometric (GM) landmarks (Fig. 1, in red; Table S2), were used to describe lateral body shape. These landmarks were chosen to be easily recognizable anatomical features that provide coverage over the body while also being informative with respect to the anatomical source of shape variation. Homology constraints on landmark choice were relaxed in order to include information on the position of the soft and spiny portions of the dorsal and anal fins on the body. The landmarks for the insertions of these fins represent the first (anterior-most) spine and ray, middle spine and ray, and last (posterior-most) spine and ray. For specimens with even numbers of spines and/or rays, the "middle" spine/ray was chosen as follows: if there were 10 spines, the middle spine was the fifth spine. Landmarks were recorded from the radiographs using TPSDig2 (Rohlf 2013). These landmarks were then processed using generalized Procrustes analysis in MorphoJ (Klingenberg 2011) to isolate the variation in shape from that of body size. The resulting generalized Procrustes coordinates were exported from MorphoJ and used as inputs for further morphometric analyses. Centroid size for each specimen was also obtained from MorphoJ, and used in subsequent analyses of allometry.

Fin shape changes with behavior, and the fins are rarely extended after specimen fixation. Given this source of variation, anal, dorsal, and caudal fin shapes were parameterized according to the length of the fin (for the dorsal and anal fins) and its associated skeletal elements—either fin spines or fin rays (Fig. 1). The lengths of the dorsal and anal fin elements were recorded using ImageJ version 1.48 (Schneider et al. 2012) for each of the first, middle, and last spines and rays, as determined for the geometric landmarks, by manually fitting a spline to each fin element. Dorsal and anal fin length was measured as the length of the body curvature at the fin insertion. Cichlid caudal fins are generally homocercal, and caudal fin ray counts are very highly conserved. All of the specimens in this study possessed eight costal fin rays in the dorsal half of the caudal fin. Therefore, to parameterize shape of the caudal fin, the lengths of caudal fin rays 1, 3, 5, and 8, as counted from the dorsal caudal fin margin, were measured (Fig. 1).

Procrustes transformation of GM landmarks accounted for differences in the body size of specimens, but linear fin measurements initially do not account for body size. To account for size variation in fin length and fin element length in an attempt to isolate differences in shape, linear measurements were scaled in one of two ways. Dorsal and anal fin base lengths (along the body margin) were divided by body length, and the resulting ratio was used for subsequent analysis. To account for overall body size in the fin element lengths, the length of each fin element for each specimen was linearly regressed on specimen centroid size in R, and the residual of each specimen from these regressions was used as a size-normalized input for subsequent analyses (Fig. S3).

PHYLOGENETIC DATA AND CLADE ASSIGNMENT

There is controversy over the timescale of cichlid evolution, and even with similar topologies, comparative analyses can be very sensitive to the differences in branch length of a phylogeny. Estimates for the date of the Pseudocrenilabrinae–Cichlinae

divergence, and the diversification of African cichlids vary in the recent literature by more than 40 million years (Genner et al. 2007; Friedman et al. 2013; McMahan et al. 2013). To account for both possible timelines of cichlid evolution, all phylogenetic comparative methods in this study were performed twice: each time using a different tree. One tree, Friedman et al. (2013), proposes a short-branch-length timeline for cichlid evolution. The second tree, McMahan et al. (2013), proposes a long-branch-length timeline. The two phylogenies were both pruned using *ape* (Paradis et al. 2004) to include only those taxa for which I had morphological data. The pruned trees contained 52 and 50 species, respectively, retaining approximately half of the taxa of the original trees, and those taxa were evenly distributed over the original trees. Twenty-eight species were common to both pruned phylogenies, and for these species, the same morphological data were used for each analysis. However, the sister nodes including these species largely differed between the two pruned phylogenies.

In order to facilitate visualization of phylogenetic patterns in morphology in nonphylogenetic analyses, each specimen was assigned to a larger clade. Usually, the assignment was the cichlid tribe to which the specimen belonged (Figs. S1, S2). For neotropical species, tribe assignments were generally determined according to McMahan et al. (2013), and consistent across the recent literature (Fig. S2, Table S1). The state of African cichlid tribes, however, is in flux, and tribe assignments in the literature are inconsistent. Therefore, specimens from Africa were only grouped by tribe for noncontroversial tribes. For controversial groups, monophyletic clades from Friedman et al. (2013) were assigned numbers (Figs. S1, S2; Table S1), and specimens were assigned to one of the numbered clades. Clade assignments were determined from Friedman et al. (2013) for species represented in that phylogeny. For all other African species, a broad literature search was used to find phylogenies placing the taxa within a broader tree, and each taxon was assigned to the group of its nearest neighbor represented in the referenced phylogenies (see Table S1 and associated references for phylogenies used).

MORPHOLOGICAL VARIATION OF SINGLE STRUCTURES

To determine the amount and nature of the variation of particular structures, separate principal components analyses (PCA) were conducted for body shape, caudal fin shape, dorsal fin shape, and anal fin shape. For body shape, general Procrustes coordinates were used as the input for PCA, and for the median fins, the normalized base and fin element lengths were used. When the measurements used in PCA are of different scales, or the variance of individual variables differs greatly, PCA using the covariance matrix may lose much of its meaning (Joliffe 2002). Therefore, to mitigate the effects of using different measurements, all PCAs were conducted using correlation matrices. Only species for which the body and fins were intact in good condition were included in those analyses: if a specimen had a damaged caudal fin, it was not included in the caudal fin PCA (see Table S1 for which specimens were included in each analysis). PCAs were conducted using R base statistics. The number of PCs used to describe each structure was determined by including n PCs such that for the variance explained by PC n, $\text{var}(n) > \text{var}(n+1) \times 2$. In some cases (dorsal fin and anal fin), only one PC met this condition, but a second PC was included for the purpose of two-dimensional data visualization. Procrustes coordinates were projected into tangent space for visual analysis (Fig. 2).

Phylogenetic PCAs were conducted using *phytools* on both phylogenies to account for phylogenetic patterns in morphology from common ancestry, using the subsets of morphological data represented on the phylogenies (Revell 2009, 2012).

ANALYSES OF DISPARITY

Disparity through time (DTT) plots (Harmon et al. 2003) were generated using the R package *geiger* (Harmon et al. 2008) from the size-normalized data for each structure, using the tree data from the Friedman and the McMahan trees. Only those taxa that were included in either phylogeny were incorporated into this analysis.

PHYLOGENETIC SIGNAL AND CONVERGENCE IN CICHLID MORPHOLOGY

To determine whether there was significant phylogenetic signal in the variation of structures, K_{mult}, a multitrait measure of phylogenetic signal, was calculated for each of the four structures over both reference phylogenies following the procedure of Adams (2014) using *geomorph* (Adams and Otarola-Castillo 2013). To visually assess the extent of phylogenetic signal in cichlid morphology, phylomorphospace plots were produced from the original PCA for each phylogeny-specific dataset using *phytools* (Revell 2012).

To determine focal groups that may have been subject to convergent evolution, SURFACE analyses using the R package *surface* (Ingram and Mahler 2013) were conducted on each set of phylogenetic PC scores for the first PCs of each structure. SURFACE uses Ornstein-Uhlenbeck stabilizing selection models and stepwise Akaike Information Criterion to locate regime shifts on a tree and identify whether those shifts are towards convergent regimes (Ingram and Mahler 2013). This allows one to look for convergent regimes that best explain a given set of trait data, with no need for a priori information about focal groups. Following SURFACE analysis, groups identified as convergent by *surface* were used as input focal groups in the R package *windex* (Arbuckle and Minter 2015), to measure the strength of the convergence using the Wheatsheaf index (Arbuckle et al. 2014).

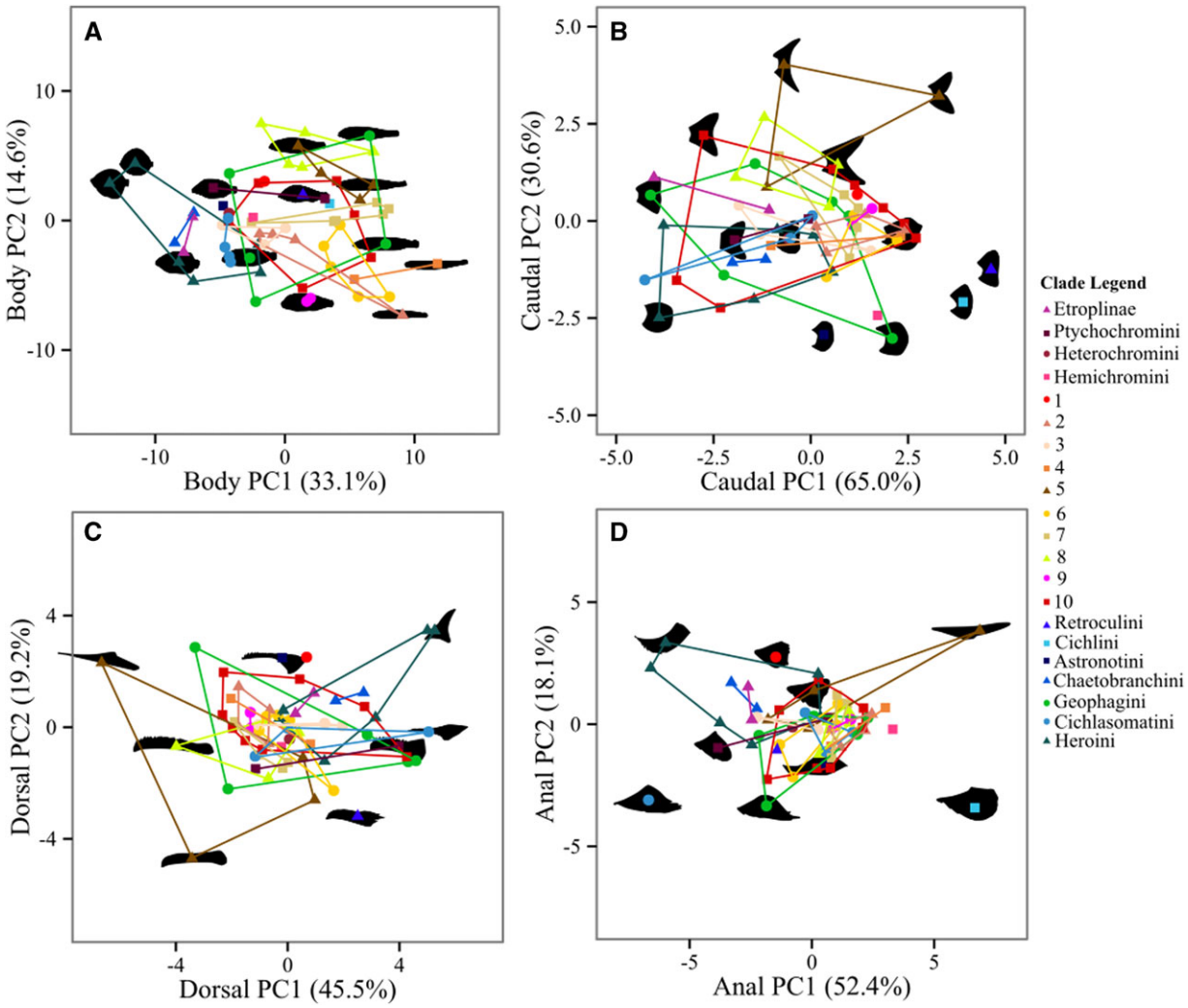

Figure 2. **Morphospace plots showing principal component scores from size-corrected traits of anatomical structures. (A) Body shape, from 27 morphological landmarks. (B) Caudal fin shape, from four lengths. (C) Dorsal fin shape, from seven lengths. (D) Anal fin shape, from seven lengths. Variance explained by each principal component is included in parentheses next to the appropriate axis label. Species silhouettes are shown centered about their point in each graph, to aid visual interpretation. Explanation of legend labels is given in the text and illustrated in Figures S1 and S2. Polygons are drawn by connecting the most extreme members of each clade.**

ANALYSIS OF MORPHOLOGICAL COVARIATION AND COEVOLUTION AMONG STRUCTURES

The principal goal of this study was to look for patterns of co-occurrence and co-evolution of particular body and fin shapes. To these ends, multiple two-block partial least-squares canonical analyses (PLS-CA) were used, treating the morphological data from each individual structure (i.e., body shape or fin shape) as a block of data. PLS-CA uses an iterative algorithm to find pairs of canonical variates (CVs), where each CV is associated with one of the two blocks of data. Each CV is selected to explain its associated data block well, and to have a high correlation with the other CV (Tenenhaus 1998). A useful feature of PLS-CA is that the data blocks provided as inputs are treated symmetrically, without implying the predictor and response relationships typical of regression-based analyses. PLS-CA is analogous to PCA in that the first pair of canonical variates explains the most covariation in the multiblock dataset. PLS-CAs were performed using the R package *plsdepot* (Sanchez 2012), which implements PLS-CA as defined in Tenenhaus (1998).

PLS-CAs were performed on the normalized trait data for all measured specimens for each two-structure pairing. Separate PLS-CAs were performed on phylogenetic independent contrasts (PICs) of the trait data for each phylogeny specific dataset. PICs were calculated using *ape* (Paradis et al. 2004). See Table S1 for which specimens were included in each analysis.

ALLOMETRIC TRENDS

While all traits in this study were size-corrected, this does not preclude the possibility of allometric trends in morphology: it is still possible for shape variation to correlate with size. In

order to identify size-linked variation in shape, linear regressions of principal component scores and centroid size were calculated (Table S3, Fig. S3). To assess the existence of allometric trends visually, centroid size was plotted on top of each structure's morphospace, which allowed for a visual assessment of the extent to which areas of morphospace were restricted to particular body size fishes (Fig. S4).

Results

MORPHOLOGICAL VARIATION OF SINGLE STRUCTURES

In cichlid fishes, the major axis of body shape variation was one of body depth (Fig. 2; PC1; Tables 2, 3). This PC explained more than 33% of the variation in cichlid body shape, with shapes ranging from deep-bodied species to those with slender lateral profiles. Notably, the GM landmarks that captured body length information did not load heavily on PC1 (Tables 2, 3). PC2 only explained ∼15% of body shape variation, and appeared to show body "truncation," distinguishing those body profiles with long heads and peduncles from those with minimal peduncle length (Tables 2, 3; Fig. 2). The clustering of taxonomic groups in body morphospace suggests that some of this shape variation may be attributable to phylogenetic constraint, but see the section below on analyses of phylogenetic signal, as well as Figures S5 and S6.

Over 95% of the variation in caudal fin shape was described by two PCs (Tables 2, 3; Fig. 2). PC1, which explained 65% of the variance in caudal fin shape, described the length of caudal fin rays relative to size (Tables 2, 3; Fig. 2). Individuals scoring highly on this PC had all four measured caudal fin rays shorter than would be predicted for their size. PC2 for caudal fin shape explained over 30% of variation in the caudal fin, and described fin concavity: specimens scoring highly on PC2 had long first and third caudal fin rays, and shorter fifth and eighth caudal fin rays (Fig. 2; Tables 2, 3). In general, this described a trend of increasing "forked appearance" of the tail along PC2.

Dorsal fin shape was best described by a single PC that explained 45% of the observed shape variation (Tables 2, 3). This PC described lengthening of the central structures of the dorsal fin—as is evidenced by the high loadings of the last dorsal fin spine, first dorsal fin ray, and middle dorsal fin ray relative to the other marginal fin elements (Fig. 2; Tables 2, 3). Dorsal fin PC2 described the tendency for fishes with longer dorsal fin bases to have short anterior fin spines, and a short posterior fin ray with respect to other fishes of their size; but PC2 only explained 19% of the variation in dorsal fin shape (Tables 2, 3).

Anal fin shape was similarly well described by a single PC, explaining 52% of that fin's observed variation (Tables 2, 3). As for the dorsal fin, anal fin PC1 described a correlated change in length across all of the fin elements measured, with highly negative loadings for the last anal fin spine, first anal fin ray, and middle anal fin ray (Fig. 2; Tables 2, 3). This similarity in loadings likely reflected the dorsoventral symmetry of median fins.

There were no obvious allometric trends in the shape of individual morphological structures (Table S3, Fig. S4). In general, larger cichlids occupied a greater proportion of the fin morphospace than smaller cichlids, but smaller cichlids occupied a

Table 2. Loadings of morphological traits on principal components.

Body shape			
Variable	PC1 (33.1%)	Variable	PC2 (14.6%)
8*y*	0.23	10*x*	–0.34
7*y*	0.23	9*x*	–0.34
22*y*	–0.22	11*x*	–0.30
18*y*	–0.22	8*x*	–0.27
6*y*	0.22	6*x*	0.22
9*y*	0.22	14*x*	0.21
17*y*	–0.21	13*x*	0.21
10*y*	0.21	7*x*	0.21
11*y*	0.21	5*x*	0.21
21*y*	–0.20	24*x*	0.21

Caudal fin		
Variable	PC1 (65.0%)	PC2 (30.6%)
Fin ray 1 (CFR1)	–0.47	0.56
Fin ray 3 (CFR3)	–0.55	0.36
Fin ray 5 (CFR5)	–0.56	–0.35
Fin ray 8 (CFR8)	–0.41	–0.66

Dorsal fin		
Variable	PC1 (45.5%)	PC2 (19.2%)
Base length (Dbase)	0.18	0.44
Fin spine 1 (DFS1)	0.01	–0.67
Fin spine mid (DFSmid)	0.40	–0.33
Fin spine last (DFSlast)	0.52	0.10
Fin ray 1 (DFR1)	0.51	0.18
Fin ray mid (DFRmid)	0.49	0.02
Fin ray last (DFRlast)	0.21	–0.44

Anal fin		
Variable	PC1 (52.4%)	PC2 (18.1%)
Base length (Abase)	–0.30	0.29
Fin spine 1 (AFS1)	–0.33	–0.20
Fin spine mid (AFSmid)	–0.46	0.09
Fin spine last (AFSlast)	–0.50	0.18
Fin ray 1 (AFR1)	–0.46	0.09
Fin ray mid (AFRmid)	–0.35	–0.45
Fin ray last (AFRlast)	–0.05	–0.79

For body shape, only the 10 variables with the highest magnitude loadings were included. For body shape variables, the number indicates the coordinate, and the letter (*x* or *y*) indicates the relevant component of the coordinate (see Fig. 1 for coordinate labels). Full listings of variable loadings can be recreated using code and data in the associated Dryad data package.

Table 3. Loadings of morphological traits on phylogenetically corrected principal components.

Body shape							
Friedman et al. (2013)				McMahan et al. (2013)			
Variable	phylPC1 (34.9%)	Variable	phylPC2 (18.1%)	Variable	phylPC1 (33.8%)	Variable	phylPC2 (25.7%)
7y	0.93	10*x*	–0.96	8y	–0.96	13*x*	–0.93
8y	0.92	9*x*	–0.96	9y	–0.95	10*x*	0.92
18y	–0.92	11*x*	–0.77	17y	0.94	9*x*	0.91
6y	0.90	8*x*	–0.70	10y	–0.94	14*x*	–0.91
22y	–0.87	14*x*	0.57	18y	0.91	27*x*	–0.87
17y	–0.86	13*x*	0.54	7y	–0.90	15*x*	–0.86
27*x*	–0.83	15*x*	0.51	22y	0.89	8*x*	0.85
16y	–0.82	27*x*	0.49	6y	–0.82	11*x*	0.80
19y	–0.81	10y	0.47	11y	–0.79	13y	0.74
9y	0.81	9y	0.45	24*x*	–0.78	4*x*	–0.60

Caudal fin				
Tree	Friedman et al. (2013)		McMahan et al. (2013)	
Variable	phylPC1 (60.5%)	phylPC2 (33.6%)	phylPC1 (68.9%)	phylPC2 (26.8%)
Fin ray 1 (CFR1)	–0.57	0.77	–0.79	0.59
Fin ray 3 (CFR3)	–0.80	0.52	–0.92	0.30
Fin ray 5 (CFR5)	–0.91	–0.34	–0.91	–0.32
Fin ray 8 (CFR8)	–0.79	–0.58	–0.79	–0.68

Dorsal fin				
Tree	Friedman et al. (2013)		McMahan et al. (2013)	
Variable	phylPC1 (73.3%)	phylPC2 (9.9%)	phylPC1 (73.7%)	phylPC2 (13.0%)
Base length (Dbase)	0.18	0.03	0.35	–0.34
Fin spine 1 (DFS1)	–0.10	–0.01	0.09	0.18
Fin spine mid (DFSmid)	0.57	–0.03	0.56	0.06
Fin spine last (DFSlast)	0.83	–0.45	0.86	–0.42
Fin ray 1 (DFR1)	0.87	–0.44	0.90	–0.36
Fin ray mid (DFRmid)	0.98	0.18	0.94	0.34
Fin ray last (DFRlast)	0.41	0.62	0.16	0.58

Anal fin				
Tree	Friedman et al. (2013)		McMahan et al. (2013)	
Variable	phylPC1 (61.3%)	phylPC2 (26.0%)	phylPC1 (73.0%)	phylPC2 (16.2%)
Base length (Abase)	0.32	–0.03	–0.40	0.32
Fin spine 1 (AFS1)	0.60	–0.22	–0.63	–0.16
Fin spine mid (AFSmid)	0.71	–0.36	–0.80	0.17
Fin spine last (AFSlast)	0.82	–0.51	–0.90	0.34
Fin ray 1 (AFR1)	0.78	–0.57	–0.90	0.35
Fin ray mid (AFRmid)	0.85	0.53	–0.87	–0.48
Fin ray last (AFRlast)	0.20	0.44	–0.32	–0.65

For body shape, only the 10 variables with the highest loadings were included. For body shape variables, the number indicates the coordinate, and the letter (*x* or *y*) indicates the horizontal or vertical component of the coordinate, respectively. Full listings of variable loadings can be recreated using code and data in the associated Dryad data package.

greater proportion of body morphospace (Fig. S4). This may be an artefact of the relative number of small cichlid species to large-bodied species in the cichlids as a group, and/or in the study sample.

PHYLOGENETIC SIGNAL IN CICHLID MORPHOLOGY

As has been found previously (Clabaut et al. 2007; Muschick et al. 2012), there is less phylogenetic signal in cichlid morphology than is predicted under a Brownian model of trait evolution,

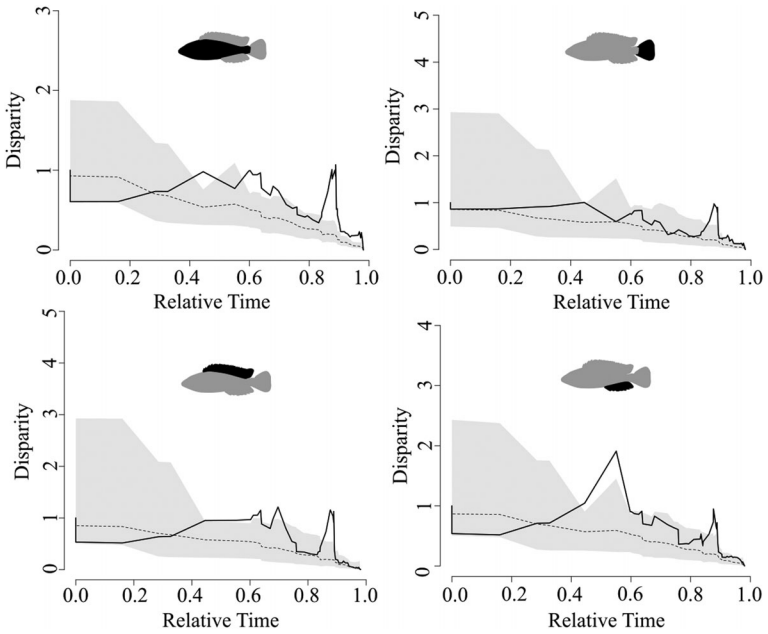

Figure 3. **Cichlid disparity through time for each anatomical structure calculated from the Friedman tree dataset (black line) with 95% confidence intervals following the method of Slater et al. (2013). Each structure is indicated in black on a silhouette. Mean expected disparity under the BM model is shown as the dotted line. Peaks above the gray confidence interval show higher disparity than expected under a BM model of trait evolution. Relative time is calculated from the tree length of the pruned subtrees specific to each morphological structure.**

though this deviation from the BM model was only significant in two out of eight cases. Across the Friedman tree dataset, K_{mult} ranged from 0.303 (for dorsal fin shape) to 0.367 (for body shape), which, while much lower than the expected $K_{\text{mult}} = 1$ for a BM model, was never significant at the $P < 0.05$ level following false detection rate correction (Benjamini and Hochberg 1995). For the McMahan tree dataset, K_{mult} ranged from 0.547 (for anal fin shape) to 0.741 (for caudal fin shape). These values were significant for anal fin and dorsal fin shape following false detection rate correction, indicating that the dorsal and the anal fins were more different among related species than expected under a BM model. This is consistent with the repeated findings that trait evolution in cichlids, be that trait diet, body shape, or pharyngeal jaw shape, is by and large independent of species' ancestral history (Clabaut et al. 2007; Muschick et al. 2012). This was visually confirmed by the phylomorphospace plots generated from each of the two cichlid phylogenies (Figs. S5, S6). There were some taxa identified as having convergent in morphology according to the SURFACE algorithm, but analyses of these focal groups in *windex* revealed no statistically significant convergence beyond that which may be expected randomly given the cichlid phylogenetic topology (Figs. S7–S10).

DISPARITY THROUGH TIME

Increases in disparity, particularly in body shape and median fin shape, paralleled increases in taxonomic diversity through time (Figs. 3, S11; Friedman et al. 2013; McMahan et al. 2013). Peaks in body and median fin disparity above that predicted by a null model of morphological evolution occur at the same time as the Cichlinae–Pseudocrenilabrinae split (as estimated by the tree from which the DTT plot was produced ~ 45 myr for analyses using the Friedman et al. [2013] data, and ~72 myr for analyses using the McMahan et al. [2013] data), and later peaks at about the same time as the haplochromine radiation (< 1 myr from the Friedman et al. 2013 data, no haplochromines were included in the McMahan et al. 2013 data).

COVARIATION OF FINS AND BODY SHAPE

Body and fin morphology in cichlids is characterized by tight covariation of structures (Figs. 4, 6, S12; Tables 4, S4, S5). The major axes of body and fin covariation as determined by PLS-CA depict linked variation that combines the major axes of variation found in the single-structure PCAs. Deep body profiles and fin length elongation (relative to body size) were always represented as the first CV pair in all of the PLS-CAs of body and fin shape (Fig. 5; Tables 4, S4, S5). The first CVs of all fin–fin analyses also reflected covariation of fin element length: fin element lengths are directly correlated—if one fin is long relative to body size, all of the fins tend to be long relative to body size (Fig. 5; Tables 4, S4, S5). In general these analyses reflect strong covariation of gross morphology, where deep-bodied fishes have long fin elements, and elongate/narrow-bodied fishes have short fin elements relative

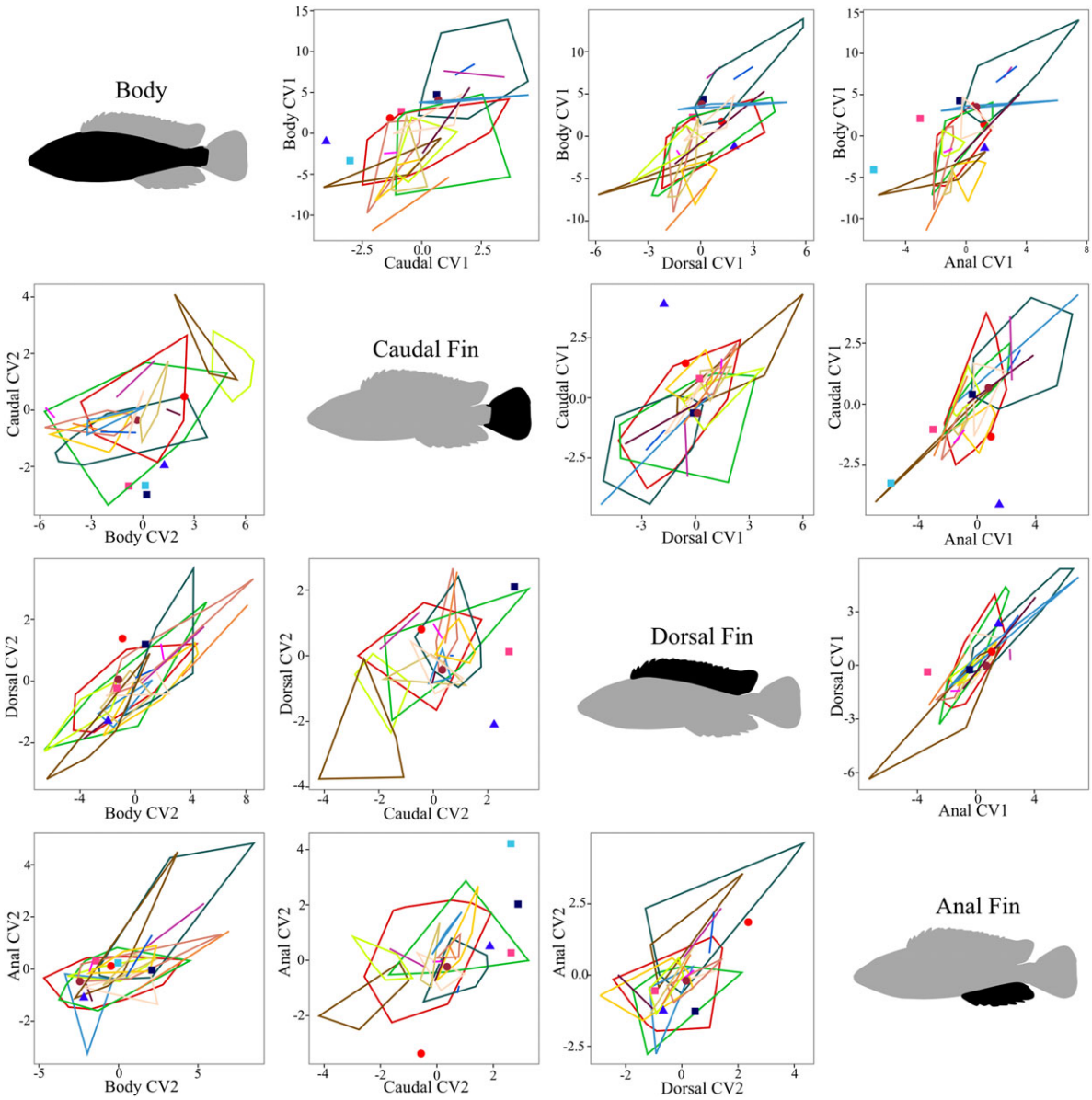

Figure 4. Partial least-squares canonical variates displaying covariation of body shape and median fin shapes across cichlid species without controlling for phylogenetic information. Polygons are drawn using line segments connecting the most extreme members of each clade, with monotypic clades represented by single points. Point color and shapes and polygon color indicate clade assignment following the key in Figures 2, S1, and S2. All of the two-structure comparisons show tight correlation between the first pair of canonical variates (described in Fig. 5 [col. A] and Table 4).

to body centroid size, with correlation coefficients between the first pairs of body–fin CVs ranging from $r = 0.48$ to $r = 0.72$ (Fig. 5; Tables 4, S4, S5). The strongest pattern of correlated evolution was that represented by the first pair of CVs describing the dorsal and anal fin ($r = 0.88$, $r = 0.84$, $r = 0.88$ in the nonphylogenetic analysis, Friedman tree analysis, and McMahan tree analysis, respectively): as the dorsal fin elements elongated, so did the anal fin elements (Figs. 4, 5; Tables 4, S4, S5).

Although the second pairs of CVs describe slightly weaker correlations (Fig. 4; Tables 4, S4, S5), they also suggest strong and functionally relevant patterns of shape covariation (Fig. 5). Unlike the first CV pairs, the second pairs also often describe changes in fin shape beyond that of lengthening or shortening of all fin elements together. In other words, for the second CV pairs, the shape changes represented result in differences in the fin margin profile, not merely fin length (Fig. 5). Notable patterns of covariation among the second CV pairs included lengthening and narrowing of the caudal peduncle with the evolution of a more forked caudal fin (Body–Caudal Fin CV2, $r = 0.52$, $r = 0.57$, $r = 0.52$ in the nonphylogenetic analysis, Friedman tree analysis, and McMahan tree analysis, respectively; Figs. 4, 5), and the

Table 4. Partial least-squares canonical variate variable loadings.

Body–caudal PLS							
First CV pair ($r = 0.61$)				Second CV pair ($r = 0.52$)			
Variable	CV1 body loading	Variable	CV1 caudal loading	Variable	CV2 body loading	Variable	CV2 caudal loading
8*y*	0.23 (92%)	CFR1	0.39 (36%)	10*x*	–0.35 (84%)	CFR1	0.68 (60%)
7*y*	0.23 (90%)	CFR3	0.50 (61%)	9*x*	–0.35 (83%)	CFR3	0.51 (34%)
22*y*	–0.22 (88%)	CFR5	0.61 (92%)	11*x*	–0.31 (67%)	CFR5	–0.16 (3%)
18*y*	–0.22 (86%)	CFR8	0.51 (64%)	8*x*	–0.28 (53%)	CFR8	–0.50 (32%)
9*y*	0.22 (86%)			6*x*	0.25 (43%)		
17*y*	–0.22 (85%)			13*x*	0.24 (39%)		
10*y*	0.22 (83%)			14*x*	0.24 (39%)		
6*y*	0.22 (83%)			5*x*	0.23 (37%)		
11*y*	0.22 (82%)			24*x*	0.23 (36%)		
21*y*	–0.21(77%)			15*x*	0.22 (35%)		
Body–dorsal PLS							
First CV pair ($r = 0.71$)				Second CV pair ($r = 0.79$)			
Variable	CV1 body loading	Variable	CV1 dorsal loading	Variable	CV2 body loading	Variable	CV2 dorsal loading
8*y*	0.23 (94%)	Dlength	0.21 (14%)	11*x*	0.31 (63%)	Dlength	0.84 (76%)
7*y*	0.23 (91%)	DFS1	–0.02 (0%)	12*x*	0.25 (42%)	DFS1	–0.36 (14%)
18*y*	–0.23 (86%)	DFSmid	0.38 (44%)	26*y*	0.25 (41%)	DFSmid	–0.33 (12%)
17*y*	–0.23 (86%)	DFSlast	0.54 (88%)	4*y*	–0.24 (37%)	DFSlast	–0.06 (0%)
9*y*	0.22 (85%)	DFR1	0.53 (88%)	9*x*	0.24 (36%)	DFR1	–0.01 (0%)
22*y*	–0.22 (85%)	DFRmid	0.49 (73%)	10*x*	0.23 (35%)	DFRmid	–0.14 (2%)
10*y*	0.22 (82%)	DFRlast	0.15 (7%)	6*x*	–0.23 (35%)	DFRlast	–0.32 (10%)
6*y*	0.22 (82%)			1*x*	0.23 (33%)		
11*y*	0.22 (79%)			7*x*	–0.22 (33%)		
21*y*	–0.21 (73%)			21*x*	0.22 (31%)		

(*Continued*)

Table 4. Continued.

Body–anal PLS							
First CV pair ($r = 0.72$)				Second CV pair ($r = 0.64$)			
Variable	CV1 body loading	Variable	CV1 anal loading	Variable	CV2 body loading	Variable	CV2 anal loading
8*y*	0.23 (91%)	Alength	0.36 (44%)	26*y*	0.32 (55%)	Alength	0.63 (44%)
7*y*	0.23 (88%)	AFS1	0.29 (30%)	1*x*	0.28 (41%)	AFS1	–0.61 (41%)
18*y*	–0.23 (87%)	AFSmid	0.45 (70%)	12*x*	0.28 (40%)	AFSmid	–0.24 (6%)
17*y*	–0.23 (87%)	AFSlast	0.51 (90%)	4*y*	–0.27 (39%)	AFSlast	0.02 (0%)
22*y*	–0.23 (87%)	AFR1	0.48 (81%)	5*y*	–0.24 (30%)	AFR1	0.04 (0%)
9*y*	0.22 (83%)	AFRmid	0.36 (47%)	3*y*	–0.23 (27%)	AFRmid	–0.28 (9%)
10*y*	0.22 (81%)	AFRlast	0.05 (1%)	25*x*	–0.22 (26%)	AFRlast	–0.35 (14%)
6*y*	0.22 (80%)			26*x*	–0.22 (25%)		
11*y*	0.22 (80%)			18*x*	–0.22 (25%)		
21*y*	–0.21 (77%)			21*x*	–0.21 (24%)		
Caudal–dorsal PLS							
First CV pair ($r = 0.69$)				Second CV pair ($r = 0.38$)			
Variable	CV1 caudal loading	Variable	CV1 dorsal loading	Variable	CV2 caudal loading	Variable	CV2 dorsal loading
CFR1	–0.36 (31%)	Dlength	–0.13 (5%)	CFR1	–0.70 (65%)	Dlength	0.76 (56%)
CFR3	–0.49 (58%)	DFS1	0.02 (0%)	CFR3	–0.53 (37%)	DFS1	–0.64 (40%)
CFR5	–0.62 (93%)	DFSmid	–0.39 (46%)	CFR5	0.12 (2%)	DFSmid	–0.33 (10%)
CFR8	–0.53 (68%)	DFSlast	–0.53 (84%)	CFR8	0.46 (28%)	DFSlast	–0.04 (0%)
		DFR1	–0.53 (85%)			DFR1	0.06 (0%)
		DFRmid	–0.52 (81%)			DFRmid	0.08 (1%)
		DFRlast	–0.22 (14%)			DFRlast	0.05 (0%)

(*Continued*)

Table 4. Continued.

Caudal–anal PLS							
First CV pair ($r = 0.72$)				Second CV pair ($r = 0.39$)			
Variable	CV1 caudal loading	Variable	CV1 anal loading	Variable	CV2 caudal loading	Variable	CV2 anal loading
CFR1	0.39 (38%)	Alength	0.30 (32%)	CFR1	–0.67 (57%)	Alength	–0.05 (0%)
CFR3	0.51 (64%)	AFS1	0.33 (39%)	CFR3	–0.50 (31%)	AFS1	–0.01 (0%)
CFR5	0.60 (91%)	AFSmid	0.45 (73%)	CFR5	0.19 (5%)	AFSmid	–0.23 (6%)
CFR8	0.49 (60%)	AFSlast	0.49 (86%)	CFR8	0.53 (35%)	AFSlast	–0.25 (7%)
		AFR1	0.47 (78%)			AFR1	–0.16 (3%)
		AFRmid	0.39 (54%)			AFRmid	0.40 (19%)
		AFRlast	0.08 (2%)			AFRlast	0.87 (87%)
Dorsal–anal P LS							
First CV pair ($r = 0.88$)				Second CV pair ($r = 0.64$)			
Variable	CV1 dorsal loading	Variable	CV1 anal loading	Variable	CV2 dorsal loading	Variable	CV2 anal loading
Dlength	0.16 (8%)	Alength	0.30 (32%)	Dlength	0.58 (36%)	Alength	0.52 (32%)
DFS1	0.02 (0%)	AFS1	0.31 (34%)	DFS1	–0.29 (9%)	AFS1	–0.25 (8%)
DFSmid	0.40 (50%)	AFSmid	0.45 (72%)	DFSmid	–0.19 (4%)	AFSmid	0.04 (0%)
DFSlast	0.53 (87%)	AFSlast	0.49 (87%)	DFSlast	0.17 (3%)	AFSlast	0.23 (6%)
DFR1	0.52 (85%)	AFR1	0.46 (76%)	DFR1	0.17 (3%)	AFR1	0.18 (4%)
DFRmid	0.48 (73%)	AFRmid	0.39 (55%)	DFRmid	–0.23 (6%)	AFRmid	–0.38 (17%)
DFRlast	0.19 (11%)	AFRlast	0.13 (6%)	DFRlast	–0.73 (57%)	AFRlast	–0.69 (58%)

Loadings are followed by the amount of variance in each variable explained by the canonical variate (for second canonical variate pairs, this is reported as the cumulative variation explained by CV pairs 1 and 2, less the variation explained by CV pair 1). For PLS including body shape data, only the 10 body shape variables with the greatest magnitude loadings are reported. (Full statistical output can be recreated using code and data in the associated Dryad package.) Correlation coefficients relating each pair of partial least square canonical variates are reported in parentheses.

shortening of dorsal and anal fin terminal fin elements as the fin bases lengthened (Dorsal–Anal Fin CV2, $r = 0.64$; Figs. 4, 5).

As with evolutionary patterns of single structure variation, the correlated evolutionary changes in each two-structure pairing mirrored the patterns observed in the analyses that did not explicitly include phylogenetic information (Tables S4, S5). PLS-CAs of PICs of body and fin measures revealed that the evolution of deeper body profiles in cichlids co-occurred with the evolution of longer fins relative to body size; and the evolution of shallower body profiles was accompanied by the evolution of shorter fins (Tables S4, S5). In addition, the evolution of narrow, elongate caudal peduncles corresponded with the evolution of a shorter dorsal fin base, and the evolution of a more concave, forked tail (Tables S4, S5).

Discussion

An underlying assumption of fish swimming biomechanics is the existence of trade-offs in locomotor performance, resulting in selection for specialist forms that excel in certain aspects of locomotor performance to the exclusion of others. There are forms associated with economical cruising, with maximizing burst acceleration, and with execution of tight maneuvers. No single form is considered optimal for all aspects of swimming performance. The proposed prevalence of specialist forms raises the hypothesis that functional structures of locomotor morphology, the fins and the body, should vary between specialized forms. Either these structures should exhibit correlated evolution toward configurations beneficial for locomotor specialization, or retain generalist morphology with no one feature overspecialized compared to others.

Body shape disparity among the cichlid fishes has been studied extensively, repeatedly demonstrating common axes of diversification across many lineages, including the tropheines (Wanek and Sturmbauer 2015), geophagines (Astudillo-Clavijo et al. 2015), and others (Clabaut et al. 2007; Muschick et al. 2012). In most lineages the chief axis of body shape diversification was one of body depth, spanning from elongate narrow-bodied forms to deep-bodied, rounded forms; in the one exception (Wanek and Sturmbauer 2015), body depth variation still explained a substantial amount of morphological variation. While body shape is one of the chief factors governing swimming performance, fins and bodies interact in tandem when fishes swim. Despite the wealth of knowledge concerning body shape evolution in the cichlids, little is known about how the fins vary across the clade, or how fin morphology relates to body morphology. The present study demonstrates that body shape evolution does not occur independently of the fins, but rather among a suite of morphological changes that potentially augment body shape's contribution to locomotor specialization.

BODY AND FIN SHAPE VARIATION ENCOMPASSES SPECIALIST FORMS

PCAs of fin and body shape reflect the hypothesized specializations of each structure, with morphological variation of the fins and the bodies falling on spectra that span between specialized forms (Fig. 2). More than 33% of the variation in body shape was explained by differences in body depth (Fig. 2, Table 3), which is frequently associated with trade-offs in pelagic versus littoral habits. Specifically, streamlined forms are considered adaptive for economical open water swimming (pelagic), whereas deep-bodied forms are considered specialists for maneuverability in structurally complex environments (littoral). The association between deep-bodied forms and maneuvering performance, and slender-bodied forms and cruising performance has been demonstrated in a few studies (Ohlberger et al. 2006; Ellerby and Gerry 2011); though some studies reveal little relationship between body shape and swimming performance (Webb et al. 1996; Gerstner 1999).

Most of the variation in cichlid caudal fins was explained by a single axis ranging from fishes with long caudal fin elements to fishes with short caudal fin elements relative to body size (Fig. 2, CPC1; Table 3). Typically, long, high-surface-area fins are associated with maneuvering performance, and this axis may in part distinguish maneuvering specialists. Greater than 30% of the variation in caudal fins reflected the spectrum between forked or concave tails and convex, rounded tails. Forked tails—semilunate tails in particular—are ascribed a thrust enhancing function with minimal additional cost, a hallmark of thunniform swimmers of high economy. Broad rounded tails, on the other hand, are employed by burst accelerators to use recoil to generate high thrust (at considerable energetic cost), and by maneuverers to generate pitching moments.

It is more difficult to relate variation in the median fins to specific hydrodynamic functions, in large part due to the lack of research on median fin hydrodynamics. Prior studies suggest that the dorsal and anal fins combined produce balancing torques to support roll stability and perhaps function as a "double-tail" to produce thrust during slow-speed swimming (Drucker and Lauder 2001; Standen and Lauder 2005). Both median fins are also actively spread and manipulated during maneuvers (Standen and Lauder 2005). PCAs revealed a general trend with dorsal and anal fins both ranging from forms with longer anterior spines and shorter rays, to forms with shorter spines but greatly elongated central and posterior rays (Fig. 2, Table 3). In terms of locomotor specialization, this may indicate a spectrum between short-finned but spiny forms for high-speed cruising, in which the median fins are typically collapsed, and lower speed maneuverers that may benefit from high fin surface area. For the haplochromine cichlids, it is possible that specialization or constraint of anal fin morphology is related to sexual selection for the tribe's

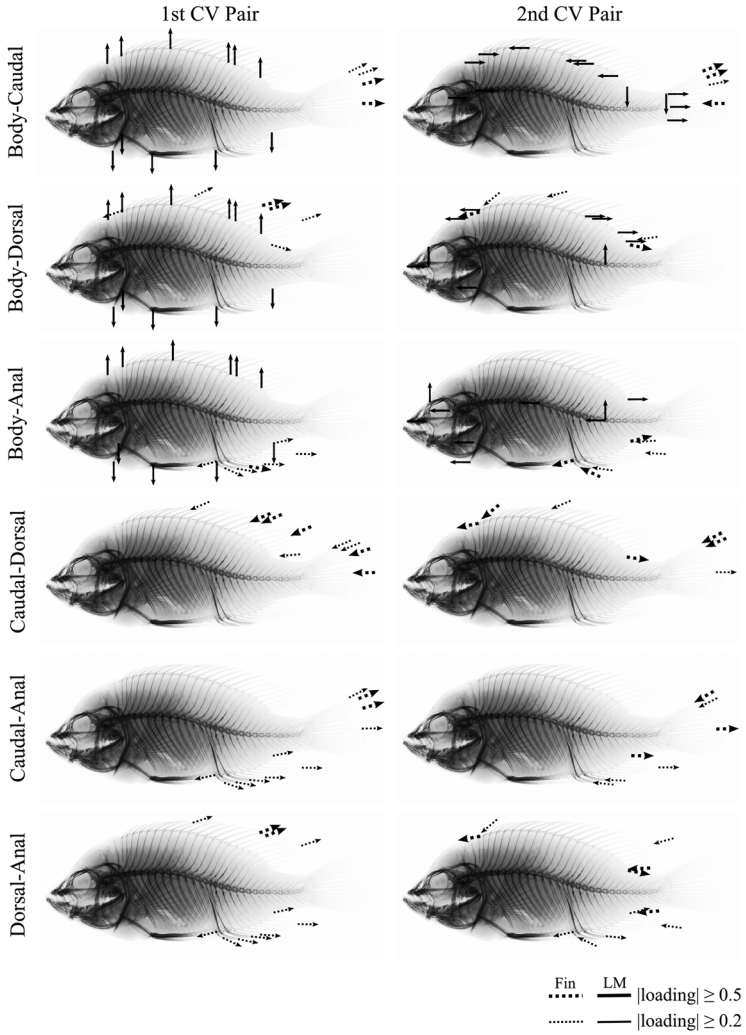

Figure 5. **Schematic depiction of partial least-squares canonical variate loadings of covarying features on a representative haplochromine cichlid (MCZ 131287 *Neochromis greenwoodi*). First canonical variate pairs exhibited the strongest covariation, while only some of the second canonical variate pairs were significant. Arrows indicate the direction of the loadings: solid arrows indicate spatial movement of geometric landmarks, and dashed arrows indicate lengthening or shortening of fin elements. Arrow thickness indicates the strength of the loading: thin arrows indicate a loading of magnitude greater than 0.2 but less than 0.5, and thick arrows indicate a loading of 0.5 or greater. The strongest relationships were between body depth and fin length. The first pairs of canonical variates (left column) show that as body depth increases, all three median fins get longer, and that all median fins tend to lengthen together.**

distinctive egg spots on the distal anal fin (Goldschmidt 2010). The probability for sexual or other selection to confound the selective pressures of locomotor performance may be higher in the median fins than in the body or the caudal fin because these fins can be almost entirely collapsed in most species. The extent to which the median fins are shaped by locomotor demands is probably modulated by the extent to which these fins are employed in swimming relative to their importance in other behaviors.

In cichlids, variation in individual locomotor structures can be explained well by merely one or two PC axes. Variation along a spectrum between implied locomotor specializations forms a major proportion of the total variation in each structure, especially for the fins. In other words, cichlid fins are either characteristic of locomotor specialization or generalists, and there are few unexpected fin morphologies.

FEATURES ASSOCIATED WITH LOCOMOTOR SPECIALIZATIONS EXHIBIT CORRELATED EVOLUTION

There was little support for either of the two null hypotheses presented for cichlid morphological evolution (Table 1). Strong correlated evolution across structures contradicted the hypothesis of complete modularity between the fins and the body (null hypothesis 1, Table 1); but the correlations between structures were not perfect, and varied in their ability to explain each structure's morphology, invalidating null hypothesis 2, though

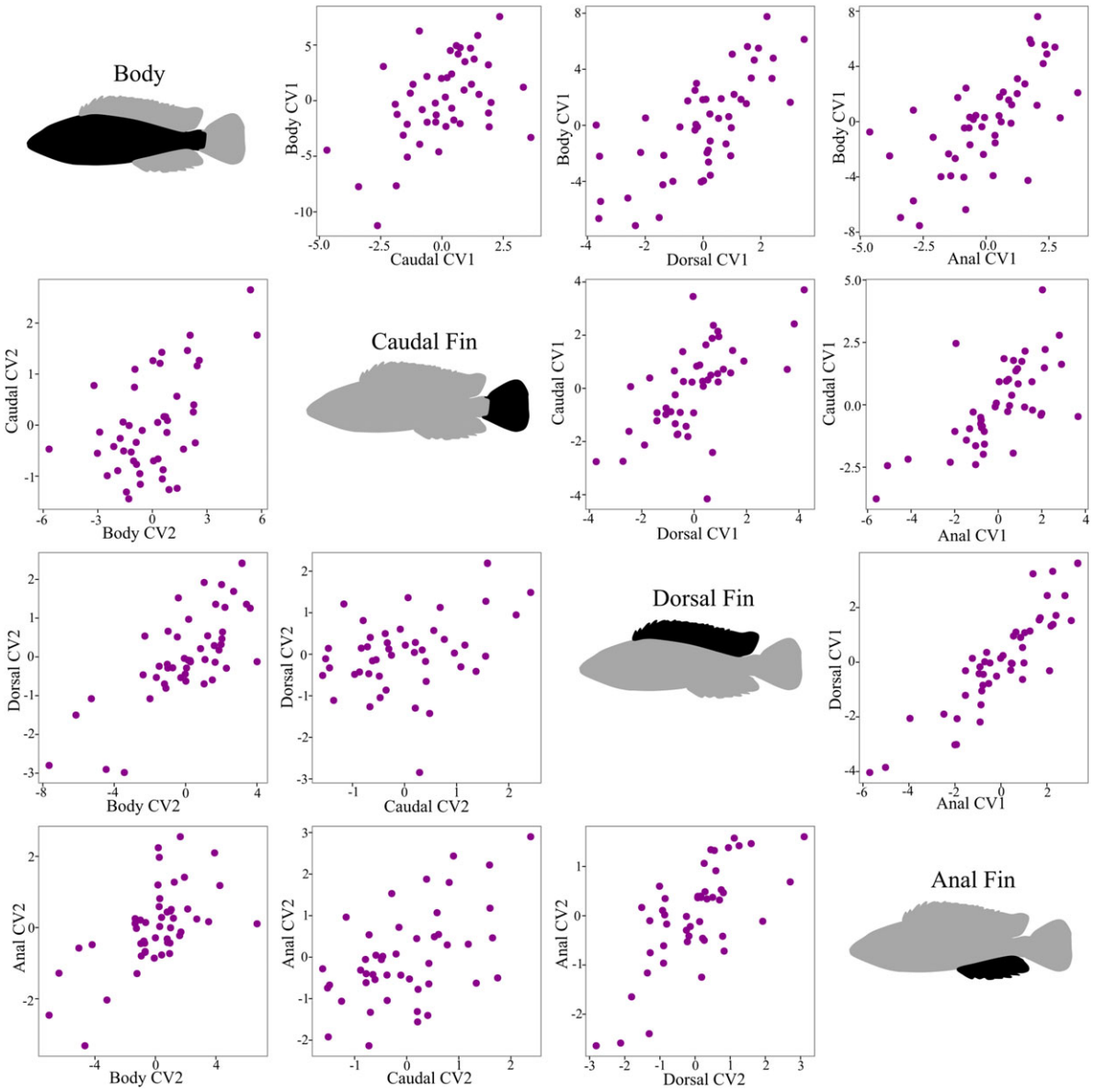

Figure 6. **Partial least-squares canonical variates displaying covariation of independent contrasts of body and median fin shapes on the McMahan et al. (2013) phylogeny.**

to a lesser degree. In contrast, and in accordance with earlier studies of ecomorphology (following Webb 1984), the correlated change of structures appears to support locomotor specialization as described by three of the four functional-linkage hypotheses in Table 1. Changes in the caudal peduncle region of the body are associated with changes in tail morphology, such that elongate, tapered peduncles co-occur with concave, forked, or semilunate tails (Tables 1 [Link 1, Body–Caudal CV2], 4, S4, S5; Figs. 4–6, S12). Median fin morphology was very strongly linked, (Tables 1 [Link 2, Dorsal-Anal CV1 and CV2], 4, S4, S5; Figs. 4–6, S12). Changes in body depth are accompanied by changes in median fin length, such that deep-bodied fishes tend to have longer fins, and elongate fishes tend to have shorter fins, relative to body size (Table 1 [Link 4; Body–Dorsal, Body–Anal CV1], 4, S4, S5; Figs. 4–6, S12). In general, these patterns are analogous to the single structure cases presented above (Figure 2): just as most individual structures vary between expected specialist forms and generalist forms with few anomalies, there are also few anomalous combinations of structures. Specialist fins are generally accompanied by appropriate specialist bodies, and generalist fins are typically accompanied by generalist bodies; with evolution toward morphological specializations occurring

repeatedly throughout the cichlid phylogeny. There are few cichlid species with combinations of body shapes associated with one specialization and fins associated with a different specialization.

The underlying pattern of morphological integration among cichlids, in which functionally linked structures evolve in tight correspondence with each other, raises the possibility that correlated evolution of structures is typical of, or even characteristic of adaptive radiation. The study of triggerfish body and fin shape (Dornberg et al. 2011) suggests that this may the case in fishes, though to generalize this across fishes requires further study. Other taxa, while more remote from fishes, also demonstrate that adaptive radiation is associated with predictable patterns of correlated evolution in suites of functionally related structures. In the lizard genus *Anolis*, for example, habitat-specific ecomorphs show correlated body, leg length, and tail length evolution: the ecomorphs are not defined by single structure modification (Losos, 1990, 1992; Mahler et al. 2010). Similar patterns of ecomorphological multitrait change have been described in frogs (Blackburn et al. 2013). If patterns of covarying morphology are constrained by or adaptive for locomotor function, perhaps other aspects of morphology and physiology also change together to support locomotion. The evidence from Lake Tanganyika showing that trophic niche, pharyngeal jaw structure, and body shape are all interrelated suggests a broad link among ecology, locomotor habits, and gross morphology (Muschick et al. 2012). While covariation of morphology and ecological niche does not necessarily ascribe a given trait change adaptive value, it does strongly suggest that natural selection acts on both ecology and morphology together. Further research into the biomechanical means by which body and fin morphology affect swimming performance is necessary to bridge the morphology–performance gap, let alone determine the consequences of morphological correlations on fitness. Nevertheless, the tightly correlated nature of cichlids' multistructure morphological evolution reflects an underlying principle of functional morphology: organisms function as integrated units, and structures must covary to function together within the context of the organism.

CICHLID MORPHOLOGY IS DICTATED BY NEITHER ANCESTRY NOR CONVERGENCE

The fact that cichlid morphology is overdispersed relative to a BM model could suggest either that cichlid morphology is not restricted by ancestry, or that there is strong convergent evolution toward optimal forms. This is also supported by the finding that the major axes of evolutionary morphological diversification in cichlids parallel the axes of morphological variation determined in the absence of phylogenetic information (Table 3). However, there was no evidence of convergent evolution beyond that expected under random BM evolution (Figs. S7–S10). This suggests that the diversity observed is not driven by shared ancestry following a single early diversification, nor by evolution toward particular optimal forms, but rather that the same trajectories of morphological evolution have occurred repeatedly across the cichlid phylogeny without reaching the same end point. The trends of varying body depth, relative fin length, and fin concavity characterize morphological disparity throughout cichlid evolution, and regions of morphospace that are empty may be so due to selection against deleterious configurations. Alternatively, common trajectories of morphological evolution may be dictated by canalized developmental linkages across structures. This is likely true for median fin shape, where there are known symmetries in the development of those structures (Mabee et al. 2002).

DIVERSIFICATION OF LOCOMOTOR STRUCTURES COINCIDES WITH ADAPTIVE RADIATION AND SPECIATION

DTT plots for body shape and all three fins exhibit peaks above the 95% confidence interval for a neutral model of BM evolution around 45 myr for both phylogenetic datasets, and around 5 myr for the Friedman dataset (Figs. 3, S11). These dates correspond loosely with the divergence of Cichlinae and Pseudocrenilabrinae (Friedman et al. 2013; McMahan et al. 2013) and the explosive radiation of the haplochromine cichlids (Genner et al. 2007; Friedman et al. 2013), respectively. The McMahan dataset only included a single haplochromine, and would not be expected to show diversification within that group. Both DTT analyses indicate that peaks in disparity occurred after major events in the biogeographic history of cichlids (such as possible vicariance or dispersal), but before any desiccation events that may have contributed to the speciation of haplochromines in Lake Victoria (Vences et al. 2001; Seehausen 2002)—which would explain the low disparity of the haplochromines compared to other groups.

The coincidence of speciation and morphological diversification reinforces the importance of morphology in adaptive radiations either as a result of species radiation, or a driver of speciation. Morphological diversification occurs concurrently with species radiation in fishes (Rabosky et al. 2013). The fact that all four structures studied displayed increased disparity at simultaneous points in time also suggests that morphological diversification occurs across structures simultaneously. This interpretation is consistent with similar findings in studies looking at body profile and pharyngeal jaw morphology in cichlids (Muschick et al. 2012).

The patterns of disparity through time indicate two major characteristics of the cichlid radiation. First, the simultaneous diversification of all locomotor structures suggests that it is unlikely that any one structure acts as a "key innovation" of locomotor morphology to release the others—or, if any structure did act as a morphological release, that the subsequent diversification of other structures happened over a short period of evolutionary time.

Second, the correspondence of changes in locomotor structures with both species radiation and diversification of trophic structures demonstrates that the adaptive radiation of cichlids was holistic, incorporating morphological diversification in structures beyond those strictly associated with feeding behavior and trophic niche.

FUNCTIONAL IMPLICATIONS OF CORRELATED EVOLUTION

The inferred patterns of correlated morphological evolution observed raise potential functional roles for correlated variation that may serve as the basis for selection for specific configurations as they affect locomotor performance. Biomechanical hypotheses and convergent morphological trajectories of distantly related lineages suggest that economical cruisers, burst accelerators, and maneuvering specialists each require a different suite of morphological traits to be most effective at their specialization (Webb 1982, 1984; Astudillo-Clavijo et al. 2015), but few studies have looked at correlated evolution of body and fin shape (save Wright 2000 and Dornburg et al. 2011 for such an analysis of triggerfishes). This study demonstrates correlated evolution of multiple locomotor traits in a macroevolutionary context, showing that these patterns are consistent with ecomorphological hypotheses.

Deep-bodied profiles with long fins, in accordance with linkage hypotheses 2 and 4, are thought to support maneuverability, providing long lever arms that can produce large turning moments. Similarly, the co-occurrence of narrow caudal peduncles and forked tails (following linkage hypothesis 1) is believed to support economical cruising, reducing drag and inertial recoil while potentially augmenting thrust. If the evolution of locomotor structures supports locomotor specialties as predicted, a nontrivial assumption given the increasing evidence of "many-to-one" mappings of morphology on performance (Wainwright et al. 2005; Collar and Wainwright 2006; Wainwright 2007), one would expect that swimming performance changes in accordance with multistructure morphology. Hence, measuring performance in phylogenetic context should be a means of testing the hypothesis that patterns of correlated morphological evolution support locomotor specialization.

The patterns presented here propose specific, testable hypotheses about performance benefits that may be accrued due to morphological covariation. For economical cruising, a narrow, elongate caudal peduncle may require a forked caudal fin to maintain thrust while reducing energetic costs. For a quick acceleration, a rounded torpedo-shaped body may be insufficient for thrust production without large median and caudal fins. Future research could determine whether the observed combinations of traits result in their hypothesized outcomes. For linkage hypothesis 1, one would expect lower cost of transport at high speeds for fishes with narrow caudal peduncles and forked tails, perhaps by hydrodynamic development of leading edge vorticity and wake recapture. For linkage hypotheses 2 and 4, one would expect fishes with deep bodies and long median fins to exhibit high maneuverability, either in terms of small turning radius or high agility. Comparison of actual performance measures, with respect to economical swimming (e.g., maximum sustainable speed, cost of transport), acceleration (e.g., maximum accelerations), and maneuvering (e.g., angular accelerations) will aid in efforts to determine whether morphological specialists exhibit performance tradeoffs in accordance with assumptions about locomotor specialization.

In conclusion, body shape does not evolve in isolation of other traits. Rather, morphological evolution in the cichlids is characterized by correlated change across a spectrum of traits that likely contribute to differences in performance and life history. These findings call for a more nuanced appreciation of both the processes of morphological evolution and development as to how correlated change comes about, and the biomechanics underlying swimming ecomorphology. In the case of cichlid morphological evolution, both the body and the fins change together, likely supporting locomotor specialization, in a pattern of tight multistructural correlation that may be the norm for adaptive trait evolution.

ACKNOWLEDGMENTS

This project was supported by a Robert A. Chapman fellowship from Harvard MCZ, and an NSF-GRF under grant DGE-1144152 to KLF. I thank G. Lauder, C. Kenaley, K. Lucas, D. Navon, J. Denton, and two anonymous reviewers for incredibly thorough and helpful discussions and comments on earlier versions of this article, and K. Hartel and A. Williston for their assistance. The author declares no conflicts of interest.

DATA ARCHIVING

Copies of MCZ specimen radiographs have been published online at MCZbase, (http://www.mczbase.mcz.harvard.edu). Morphometric coordinates, measurements, and code have been uploaded to Data Dryad Digital Repository: http://doi.org/10.5061/dryad.h4k6f.

LITERATURE CITED

Adams, D. C. 2014. A generalized K statistic for estimating phylogenetic signal from shape and other high-dimensional multivariate data. Syst. Biol. 63:685–697.

Adams, D. C., and E. Otarola-Castillo. 2013. Geomorph: an R package for the collection and analysis of geometric morphometric shape data. Methods Ecol. Evol. 4:393–399.

Affleck, R. J. 1950. Some points in the function, development, and evolution of the tail in fishes. Proc. Zool. Soc. Lond. 120:349–368.

Albertson, R. C., J. A. Markert, P. D. Danley, and T. D. Kocher. 1999. Phylogeny of a rapidly evolving clade: the cichlid fishes of Lake Malawi, East Africa. Proc. Natl. Acad. Sci. USA 96:5107–5110.

Albertson, R. C., J. T. Streelman, and T. D. Kocher. 2003. Directional selection has shaped the oral jaws of Lake Malawi cichlid fishes. Proc. Natl. Acad. Sci. USA 100:5252–5257.

Akhtar, I., R. Mittal, G. V. Lauder, and E. Drucker. 2007. Hydrodynamics of a biologically inspired tandem flapping foil configuration. Theor. Comput. Fluid Dyn. 21:155–170.

Antonucci, F., C. Costa, J. Aguzzi, and S. Cataudella. 2009. Ecomorphology of morpho-functional relationships in the family of Sparidae: a quantitative statistic approach. J. Morphol. 270:843–855.

Arbour, J. H., and H. Lopez-Fernandez. 2014. Adaptive landscape and functional diversity of Neotropical cichlids: implications for the ecology and evolution of Cichlinae (Cichlidae; Cichliformes). J. Evol. Biol. 27:2431–2442.

Arbuckle, K., and A. Minter. 2015. windex: analyzing convergent evolution using the Wheatsheaf Index in R. Evol. Bioinform. Online 11:11–14.

Arbuckle, K., C. M. Bennett, and M. P. Speed. 2014. A simple measure of the strength of convergent evolution. Methods Ecol. Evol. 5:685–693.

Astudillo-Clavijo, V., J. H. Arbour, and H. Lopez-Fernandez. 2015. Selection towards different adaptive optima drove the early diversification of locomotor phenotypes in the radiation of Neotropical geophagine cichlids. BMC Evol. Biol. 15:77.

Benjamini, Y., and Y. Hochberg. 1995. Controlling the false discovery rate: a practical and powerful approach to multiple testing. J. R. Stat. Soc. Ser. B 57:289–300.

Blackburn, D. C., C. D. Siler, A. C. Diesmos, J. A. McGuire, D. C. Cannatella, and R. M. Brown. 2013. An adaptive radiation of frogs in a southeast Asian island archipelago. Evolution 67:2631–2646.

Blake, R. W., J. Li, and K. H. S. Chan. 2009. Swimming in four goldfish *Carassius auratus* morphotypes: understanding functional design and performance employing artificially selected forms. J. Fish Biol. 75:591–617.

Borazjani, I., and M. Daghoogi. 2013. The fish tail motion forms an attached leading edge vortex. Proc. R. Soc. Lond. B 280:20122071.

Chakrabarty, P. 2005. Testing conjectures about morphological diversity in cichlids of Lakes Malawi and Tanganyika. Coepia 2005:359–373.

Clabaut, C., P. M. E. Bunje, W. Salzburger, and A. Meyer. 2007. Geometric morphometric analyses provide evidence for the adaptive character of the Tanganyikan cichlid fish radiations. Evolution 61:560–578.

Claverie, T., and P. C. Wainwright. 2014. A morphospace for reef fishes: elongation is the dominant axis of body shape evolution. PLoS One 9:e112732.

Collar, D. C., and P. C. Wainwright. 2006. Discordance between morphological and mechanical diversity in the feeding mechanism of centrarchid fishes. Evolution. 60:2575–2584.

Dornburg, A., B. Sidlauskas, F. Santini, L. Sorenson, T. J. Near, and M. E. Alfaro. 2011. The influence of an innovative locomotor strategy on the phenotypic diversification of triggerfish (Family: Balistidae). Evolution 65–67:1912–1926.

Drucker, E. G., and G. V. Lauder. 2001. Locomotor function of the dorsal fin in teleost fishes: experimental analysis of wake forces in sunfish. J. Exp. Biol. 204:2943–2958.

Ehlinger, T. J., and D. S. Wilson. 1988. Complex foraging polymorphism in bluegill sunfish. Proc. Natl. Acad. Sci. USA 85:1878–1882.

Ellerby, D. J., and S. P. Gerry. 2011. Sympatric divergence and performance trade-offs of bluegill ecomorphs. Evol. Biol. 38:422–433.

Feilich, K. L., and G. V. Lauder. 2015. Passive mechanical models of fish caudal fins: effects of shape and stiffness on self-propulsion. Bioinspir. Biomim. 10:036002.

Friedman, M. 2010. Explosive morphological diversification of spiny-finned teleost fishes in the aftermath of the end-Cretaceous extinction. Proc. R. Soc. Lond. B. 277:1675–1683.

Friedman, M., B. P. Keck, A. Dornburg, R. I. Eytan, C. H. Martin, C. D. Hulsey, P. C. Wainwright, and T. J. Near. 2013a. Molecular and fossil evidence place the origin of cichlid fishes long after Gondwanan rifting. Proc. R. Soc. Lond. B. 280:20131733.

Friedman, M., B. P. Keck, A. Dornburg, R. I. Eytan, C. H. Martin, C. D. Hulsey, P. C. Wainwright, and T. J. Near. 2013b. Data from: molecular and fossil evidence place the origin of cichlid fishes long after Gondwanan rifting. Dryad Digital Repository. doi:10.5061/dryad.48f62.

Genner, M. J., O. Seehausen, D. H. Lunt, D. A. Joyce, P. W. Shaw, G. R. Carvalho, and G. F. Turner. 2007. Age of cichlids: new dates for ancient lake fish radiations. Mol. Biol. Evol. 24:1269–1282.

Gerstner, C. L. 1999. Maneuverability of four species of coral reef fish that differ in body and pectoral-fin morphology. Can. J. Zool. 77:1102–1110.

Goldschmidt, T. 2010. Egg mimics in Haplochromine cichlids (Pisces, Perciformes) from Lake Victoria. Ethology 88:177–190.

Harmon, L. J., J. A. Schulte II, A. Larson, and J. B. Losos. 2003. Tempo and mode of evolutionary radiation in iguanian lizards. Science 301:961–964.

Harmon, L. J., J. T. Weir, C. D. Brock, R. E. Glor, and W. Challenger. 2008. GEIGER: investigating evolutionary radiations. Bioinformatics 24:129–131.

Ingram, T., and D. L. Mahler. 2013. SURFACE: detecting convergent evolution from comparative data by fitting Ornstein-Uhlenbeck models with stepwise Akaike Information Criterion. Methods Ecol. Evol. 4:416–425.

Joliffe, I. T. 2002. Principal components analysis. 2nd ed. Springer-Verlag, New York.

Klingenberg, C. P. 2011. MorphoJ: an integrated software package for geometric morphometrics. Mol. Ecol. Resour. 11:353–357.

Kocher, T. D., J. A. Conroy, K. R. McKaye, and J. R. Stauffer. 1993. Similar morphologies of cichlid fish in lakes Tanganyika and Malawi are due to convergence. Mol. Phylogenet. Evol. 2:158–165.

Kusche, H., H. Recknagel, K. R. Elmer, and A. Meyer. 2014. Crater lake cichlids specialize along the benthic-limnetic axis. Ecol. Evol. 4:1127–1139.

Lai, Y.-C. 1963. Effects of several preservatives on proportional measurement of the fat-headed minnow, Pimephales promelas. M.A. thesis, University of Kansas, Lawrence, KS.

Lauder, G. V., and E. G. Drucker. 2004. Morphology and experimental hydrodynamics of fish fin control surfaces. IEEE J. Ocean. Eng. 29:556–571.

Lauder, G. V., J. C. Nauen, and E. G. Drucker. 2002. Experimental hydrodynamics and evolution: function of median fins in ray-finned fishes. Integr. Comp. Biol. 42:1009–1017.

Lauder, G. V., B. Flammang, and S. Alben. 2012. Passive robotic models of propulsion by the bodies and caudal fins of fish. Integr. Comp. Biol. 52:576–587.

Liem, K. F. 1973. Evolutionary strategies and morphological innovations: cichlid pharyngeal jaws. Syst. Zool. 22:425–441.

Lighthill, M. J. 1970. Aquatic animal propulsion of high hydrodynamical efficiency. J. Fluid Mech. 44:265–301.

López-Fernández, H., K. O. Winemiller, C. Montaña, and R. L. Honeycutt. 2012. Diet-morphology correlations in the radiation of South American geophagine cichlids (Perciformes: Cichlidae: Cichlinae). PLoS One 7:e33997.

Losos, J. B. 1990. Ecomorphology, performance capability, and scaling of West Indian *Anolis* lizards: an evolutionary analysis. Ecol. Monogr. 60:369–388.

———. 1992. The evolution of convergent structure in Caribbean *Anolis* communities. Syst. Biol. 41:403–420.

Mabee, P. M., P. L. Crotwell, N. C. Bird, and A. C. Burke. 2002. Evolution of median fin modules in the axial skeleton of fishes. J. Exp. Zool. B Mol. Dev. Evol. 294:77–90.

Mahler, D. L., L. J. Revell, R. E. Glor, and J. B. Losos. 2010. Ecological opportunity and the rate of morphological evolution in the diversification of Greater Antillean anoles. Evolution 64:2731–2745.

McMahan, C. D., P. Chakrabarty, J. S. Sparks, W. L. Smith, and M. P. Davis. 2013. Temporal patterns of diversification across global cichlid biodiversity. PLoS One 8:e71162.

Montaña, C. G., K. O. Winemiller, and A. Sutton. 2014. Intercontinental comparison of fish ecomorphology: null model tests of community assembly at the patch scale in rivers. Ecol. Monogr. 84:91–107.

Muschick, M., A. Indermaur, and W. Salzburger. 2012. Convergent evolution within an adaptive radiation of cichlid fishes. Curr. Biol. 22:2362–2368.

Ohlberger, J., G. Staaks, and F. Hölker. 2006. Swimming efficiency and the influence of morphology on swimming costs in fishes. J. Comp. Physiol. B 176:17–25.

Paradis, E., J. Claude, and K. Strimmer. 2004. APE: analyses of phylogenetics and evolution in R language. Bioinformatics 20:289–290.

Rabosky, D. L., F. Santini, J. Eastman, S. A. Smith, B. Sidlauskas, J. Chang, and M. E. Alfaro. 2013. Rates of speciation and morphological evolution are correlated across the largest vertebrate radiation. Nat. Commun. 4:1958.

Revell, L. J. 2009. Size-correction and principal components for interspecific comparative studies. Evolution 63:3258-3268.

———. 2012. phytools: an R package for phylogenetic comparative biology (and other things). Methods Ecol. Evol. 3:217–223.

Rohlf F. J. 2013. tpsDig, digitize landmarks and outlines, version 2.17. Department of Ecology and Evolution, State University of New York at Stony Brook. Available at http://life.bio.sunysb.edu/morph/soft-dataacq.html. Accessed June 22, 2014.

Rüber, L., and D. C. Adams. 2001. Evolutionary convergence of body shape and trophic morphology in cichlids from Lake Tanganyika. J. Evol. Biol. 14:325–332.

Salzburger, W., T. Mack, E. Verheyen, and A. Meyer. 2005. Out of Tanganyika: genesis, explosive speciation, key-innovations and phylogeography of the haplochromine cichlid fishes. BMC Evol. Biol. 5:17.

Sanchez, G. 2012. Plsdepot: partial least squares data analysis methods. R package version 0.1.17. Available at https://cran.r-project.org/web/packages/plsdepot/index.html. Accessed August 25, 2014.

Schneider, C. A., W. S. Rasband, and K. W. Eliceiri. 2012. NIH Image to ImageJ: 25 years of image analysis. Nat. Methods 9:671–675.

Schwarzer, J., A. Lamboj, K. Langen, B. Misof, and U. K. Schliewen. 2015. Phylogeny and age of chromidotilapiine cichlids (Teleostei: Cichlidae). Hydrobiologia 748:185–199.

Seehausen, O. 2002. Patterns in fish radiation are compatible with Pleistocene desiccation of Lake Victoria and 14600 year history for its cichlid species flock. Proc. R. Soc. Lond. B 269:491–497.

Snorrason, S. S., S. Skulason, B. Jonsson, P. M. Jonasson, and H. J. Malmquist. 1994. Trophic specialization in arctic charr *Salvelinus alpinus* (Pisces; Salmonidae): morphological divergence and ontogenetic niche shifts. Biol. J. Linnean Soc. 52:1–18.

Standen, E. M., and G. V. Lauder. 2005. Dorsal and anal fin function in bluegill sunfish *Lepomis macrochirus*: three-dimensional kinematics during propulsion and maneuvering. J. Exp. Biol. 208:2753–2763.

Stauffer, J. R., N. J. Bowers, K. A. Kellogg, and K. R. McKaye. 1997. A revision of the blue-black *Pseudotropheus zebra* (Teleostei: Cichlidae) complex from Lake Malawi, Africa, with a description of a new genus and ten new species. Proc. Acad. Nat. Sci. Philadelphia 148:189–230.

Tenenhaus, M. 1998. La régression PLS: théorie et pratique. Editions Technip, Paris, France.

Thorsen, D. H., and M. W. Westneat. 2005. Diversity of pectoral fin structure and function in fishes with labriform propulsion. J. Morphol. 263:133–150.

Triantafyllou, M. S., G. S. Triantafyllou, and D. K. P. Yue. 2000. Hydrodynamics of fishlike swimming. Annu. Rev. Fluid Mech. 32:33–53.

Tytell, E. D., E. M. Standen, and G. V. Lauder. 2008. Escaping flatland: three-dimensional kinematics and hydrodynamics of median fins in fishes. J. Exp. Biol. 211:187–195.

Vences, M., J. Freyhof, R. Sonnenberg, J. Kosuch, and M. Veith. 2001. Reconciling fossils and molecules: cenozoic divergence of cichlid fishes and the biogeography of Madagascar. J. Biogeogr. 28:1091–1099.

Wainwright, P. C. 2007. Functional versus morphological diversity in macroevolution. Annu. Rev. Ecol. Evol. Syst. 38:381–401.

Wainwright, P. C., M. E. Alfaro, D. I. Bolnick, and C. D. Hulsey. 2005. Many-to-one mapping of form to function: a general principle in organismal design? Integr. Comp. Biol. 45:256–262.

Walker, J. A., and M. W. Westneat. 2002. Performance limits of labriform propulsion and correlates with fin shape and motion. J. Exp. Biol. 205:177–187.

Wanek, K. A., and C. Sturmbauer. 2015. Form, function and phylogeny: comparative morphometrics of Lake Tanganyika's cichlid tribe Tropheini. Zool. Scr. 44:362–373.

Ward, A. B., and R. S. Mehta. 2010. Axial elongation in fishes: using morphological approaches to elucidate developmental mechanisms in studying body shape. Integr. Comp. Biol. 50:1106–1119.

Webb, P. W. 1982. Locomotor patterns in the evolution of actinopterygiian fishes. Am. Zool. 22:329–342.

———. 1984. Body form, locomotion, and foraging in aquatic vertebrates. Am. Zool. 24:107–120.

Webb, P. W., G. D. LaLiberte, and A. J. Schrank. 1996. Does body and fin form affect the maneuverability of fish traversing vertical and horizontal slits? Environ. Biol. Fishes 46:7–14.

Weihs, D. 1989. Design features and mechanics of axial locomotion in fish. Am. Zool. 29:151–160.

Winemiller, K. O., L. C. Kelso-Winemiller, and A. L. Brenkert. 1995. Ecomorphological diversification and convergence in fluvial cichlid fishes. Environ. Biol. Fishes 44:235–261.

Wright, B. 2000. Form and function in aquatic flapping propulsion: morphology, kinematics, hydrodynamics, and performance of the triggerfishes (Tetraodontiformes: Balistidae). Ph. D. diss., Department of Organismal Biology and Anatomy, University of Chicago, Chicago, IL.

Young, K. A., J. Snoeks, and O. Seehausen. 2009. Morphological diversity and the roles of chance and determinism in African cichlid radiations. PLoS One 4:e4740.

Associate Editor: M. Friedman
Handling Editor: J. Conner

Supporting Information

Additional Supporting Information may be found in the online version of this article at the publisher's website:

Table S1. Specimens used, clade assignments for graphing, including referenced trees used to determine clade assignment, and the data blocks in which each specimen was included.
Table S2. List of geometric morphometric landmarks used to quantify body shape.
Table S3. Linear regression analyses of principal component scores on body (centroid) size.
Table S4. Partial least-squares canonical variate variable loadings for analyses conducted on phylogenetic independent contrasts of the Friedman tree morphological dataset.
Table S5. Partial least-squares canonical variate variable loadings for analyses conducted on phylogenetic independent contrasts of the McMahan tree morphological dataset.
Figure S1. Clade assignments based on Friedman et al. (2013).
Figure S2. Clade assignments based on McMahan et al. (2013).
Figure S3. Linear regressions of fin elements on body centroid size to calculate residuals which were then used in subsequent shape analyses.
Figure S4. Principal components of body and fin shapes colored by specimen size.
Figure S5. Phylomorphospace of specimens represented in the Friedman et al. (2013) tree, as calculated from the original PCA of all specimens.
Figure S6. Phylomorphospace of specimens represented in the McMahan et al. (2013) tree, as calculated from the original PCA of all specimens.
Figure S7. SURFACE analysis and Wheatsheaf indices with 95% confidence intervals for body shape on the Friedman (top) and McMahan (bottom) trees.
Figure S8. SURFACE analysis and Wheatsheaf indices with 95% confidence intervals for caudal shape on the Friedman (top) and McMahan (bottom) trees.
Figure S9. SURFACE analysis and Wheatsheaf indices with 95% confidence intervals for dorsal fin shape on the Friedman (top) and McMahan (bottom) trees.
Figure S10. SURFACE analysis and Wheatsheaf indices with 95% confidence intervals for anal fin shape on the Friedman (top) and McMahan (bottom) trees.
Figure S11. Cichlid disparity through time calculated from the McMahan tree dataset (black line) with 95% confidence intervals following the method of Slater et al. (2013).
Figure S12. Partial least-squares canonical variates displaying covariation of independent contrasts of body and median fin shapes on the Friedman et al. (2013) phylogeny.

Supplemental Data and Figures

Supplemental Table 1. Specimens used, clade assignments for graphing, including referenced trees used to determine clade assignment, and the data blocks in which each specimen was included. Inclusion in phylogenetic analyses is indicated by the trees on which the genus of the specimen is included. Clade reference is coded as follows: 1: Friedman et al 2013, 2: McMahan et al 2013, 3: Moran et al 1994, 4: Joyce et al 2011, 5: Salzburger et al 2005, 6: Day et al 2008, 7: Klett and Meyer 2002, 8: Allender et al 2003, 9: Schwarzer et al 2009, 10: Clabaut et al 2005, 11: Smith et al 2008, 12: Schwarzer et al 2015, 13: Seehausen et al 2003. All species without a listed clade reference were assigned by locality to the Haplochromines, and therefore to clade 10.

Species	Catalog No.	Clade	Ref	Body	Caudal	Dorsal	Anal	Ftree	Mtree
Acarichthys heckelii	MCZ90937	Geophagini	2,11	X	X	X	X		X
Acaronia nassa	MCZ34140	Cichlasomatini	2,11	X	X	X	X		X
Aequidens tetramerus	MCZ15953	Cichlasomatini	1,2,11	X		X	X	X	X
Amphilophus citrinellus	MCZ15412	Heroini	2,11	X	X	X	X		X
Apistogramma steindachneri	MCZ57339	Geophagini	2,11	X	X	X	X		X
Apistogrammoides pucallpaensis	MCZ51736	Geophagini	2,11	X	X	X	X		X
Aristochromis christyi	MCZ49522	10	3	X	X		X		
Astatoreochromis alluaudi	MCZ100525	10	2,5,6,10	X	X	X	X		X
Astatotilapia elegans	MCZ148145	10	1,3,4,5	X	X	X	X	X	
Astronotus ocellatus	MCZ57046	Astronotini	1,2,11	X	X	X	X	X	X
Aulonocara rostratum	MCZ131956	10	3,5	X		X	X		
Aulonocranus dewindti	MCZ49256	8	1,6,10	X	X	X	X	X	
Australoheros sp.	MCZ15404	Heroini	2,11	X	X	X	X		X
Bathybates fasciatus	MCZ98421	5	1,6,10	X	X	X	X	X	
Benitochromis cf. *batesii*	MCZ48132	2	1,12	X	X	X	X	X	
Benthochromis tricot	MCZ50834	7	1,6	X	X	X		X	
Biotodoma cupido	MCZ15628	Geophagini	2,11	X	X	X	X		X
Biotoecus sp.	MCZ16010	Geophagini	1,2,11	X	X	X		X	X
Boulengerochromis microlepis	MCZ32557	5	1,6	X	X	X	X	X	
Buccochromis lepturus	MCZ48900	10	3	X	X	X	X		
Bujurquina sp.	MCZ52157	Cichlasomatini	2,11	X	X	X	X		X
Callochromis pleurospilus	MCZ50826	8	6	X	X	X	X		
Caprichromis orthognathus	MCZ49461	10	3	X	X	X	X		
Caquetaia myersi	MCZ49322	Heroini	1,2,11	X	X	X	X	X	X
Cardiopharynx schoutedeni	MCZ50827	8	1,6	X	X	X	X	X	

Chaetobranchopsis orbicularis	MCZ15839	Chaetobranchini	2,11	X	X	X	X		X
Chaetobranchus semifasciatus	MCZ15704	Chaetobranchini	2,11	X	X	X	X		X
Chalinochromis brichardi	MCZ49219	6	2,6,11	X	X	X	X		X
Champsochromis caeruleus	MCZ49533	10	3	X	X	X	X		
Chilotilapia rhoadesii	MCZ131953	10	1,3	X	X	X	X	X	
Chromidotilapia guntheri	MCZ48601	2	7,12	X	X	X	X		
Cichla monoculus	MCZ15276	Cichlini	1,2,11	X	X		X	X	X
Cichlasoma urophthalmus	MCZ59665	Heroini	1,2,	X	X	X	X	X	X
Copadichromis quadrimaculatus	MCZ49518	10	3,4,5	X	X	X	X		
Corematodus taeniatus	MCZ131702	10		X	X	X	X		
Crenicichla johanna	MCZ15020	Geophagini	1,2,11	X	X	X	X	X	X
Cryptoheros cutteri	MCZ88630	Heroini	1	X	X	X	X	X	
Ctenochromis horei	MCZ49278	10	5,6,10	X	X	X	X		
Ctenopharynx intermedius	MCZ49497	10		X	X	X	X		
Cunningtonia longiventralis	MCZ49243	10	6,10	X	X	X	X		
Cyathochromis obliquidens	MCZ49440	10	3	X	X	X	X		
Cyathopharynx furcifer	MCZ50828	8	6,10	X	X	X	X		
Cyphotilapia frontosa	MCZ50837	7	1,5,6,10	X	X	X		X	
Cyrtocara moorii	MCZ96429	10	1,3,5	X	X	X	X	X	
Dicrossus maculatus	MCZ14855	Geophagini	1,2,11	X	X	X	X	X	X
Dimidiochromis compressiceps	MCZ49499	10	3,4	X	X	X	X		
Diplotaxodon argenteus	MCZ135962	10	3,4,5	X		X	X		
Docimodus johnstoni	MCZ49541	10	3	X	X	X	X		
Ectodus descampsii	MCZ32618	8	5,6,10	X	X	X	X		
Eretmodus cyanostictus	MCZ50700	9	1,5,6,10	X	X	X	X	X	
Etroplus suratensis	MCZ4306	Etroplinae	1,2,11	X	X	X	X	X	X
Geophagus altifrons	MCZ15173	Geophagini	1,2,3	X	X	X	X	X	X
Gobiocichla ethelwynnae	MCZ58052	4	1,9,11	X	X	X	X	X	X
Grammatotria lemairii	MCZ49277	8	6,10	X	X	X			
Guianacara geayi	MCZ30140	Geophagini	2,11	X	X	X	X		X
Gymnogeophagus gymnogenys	MCZ88954	Geophagini	2,11	X	X	X	X		X
Haplochromis lividus	MCZ100653	10	1,2	X	X	X	X	X	X

Hemibates stenosoma	MCZ49289	5	6	X	X	X	X		
Hemichromis fasciatus	MCZ31324	Hemichromini	1,2,11	X	X	X	X	X	X
Hemitilapia oxyrhyncha	MCZ49439	10	3	X	X	X	X		
Herichthys cyanoguttatus	MCZ15415	Heroini	2,11	X	X	X	X		X
Heroina isonycterina	MCZ49319	Heroini	11	X	X	X	X		
Heros severus	MCZ46095	Heroini	1,2,11	X	X	X	X	X	X
Heterochromis multidens	AMNH-I-241789	Heterochromini	1,2,10,11	X	X	X	X	X	X
Hypselecara temporalis	MCZ15344	Heroini	1,2,11	X	X	X	X	X	X
Julidochromis marlieri	MCZ48013	6	5,6,10	X	X	X	X		
Labeotropheus _____			3,4,8	X	X	X	X		
Laetacara flavilabris	MCZ49316	Cichlasomatini	1,2,11	X	X	X	X	X	X
Lamprologus lemairii	MCZ49222	6	1,6	X	X	X	X	X	
Lepidiolamprologus elongatus	MCZ49251	6	6	X	X	X	X		
Lestradea stappersii	MCZ32593	8	6	X	X				
Lethrinops furcifer	MCZ98601	10	3,4,5	X	X	X	X		
Limnochromis auritus	MCZ32324	7	5,6,10	X	X	X			
Limnotilapia dardennii	MCZ32584	10	1,6,10	X	X	X	X	X	
Lobochilotes labiatus	MCZ	10	5,6,10	X	X	X	X		
Maylandia aurora	MCZ98614	10	8	X	X	X	X		
Mbipia mbipi	MCZ100101	10	1,13	X	X	X	X	X	
Mesonauta festivus	MCZ90844	Heroini	1,2,11	X	X	X	X	X	X
Mylochromis sphaerodon	MCZ98605	10	3?	X	X	X	X		
Naevochromis chrysogaster	MCZ60431	10		X	X	X	X		
Nanochromis dimidiatus	MCZ50588	2	1,9,12	X	X	X	X	X	
Neochromis greenwoodi	MCZ131287	10	13	X	X	X	X		
Neolamprologus fasciatus	MCZ49250	6	1,2,6,11	X	X	X	X	X	X
Nimbochromis polystigma	MCZ135963	10	3,4	X	X	X	X		
Nyassachromis leuciscus	MCZ131954	10		X	X	X	X		
Ophthalmotilapia nasuta	MCZ50843	8	1,6,10	X	X	X	X	X`	
Oreochromis esculentus	MCZ100203	3	1,2,7	X	X	X	X	X	X

Otopharynx argyrosoma	MCZ131694	10	3	X	X		X		
Oxylapia polli	AMNH-I-97098	Ptychochromini	2,10	X	X	X	X		X
Parachromis managuensis	MCZ16086	Heroini	1,2,11	X	X	X	X	X	X
Parananochromis caudifasciatus	MCZ35398	2	12	X	X	X	X		
Paraneetroplus maculicauda	MCZ33281	Heroini	2,11	X	X	X	X		X
Paretroplus polyactis	MCZ165679	Etroplinae	1,2,11	X	X	X	X	X	X
Pelvicachromis pulcher	MCZ61101	2	2,7,11,12	X	X	X	X		X
Perissodus microlepis	MCZ49329	7	5,6,10	X	X		X		
Petrochromis polyodon	MCZ49233	10	1,5,6,10	X	X	X	X	X	
Placidochromis subocularis	MCZ49451	10	3,4	X	X	X	X		
Plecodus paradoxus	MCZ32594	7	1,5,6,10	X	X	X	X	X	
Protomelas triaenodon	MCZ49467	10	3,4	X	X	X	X		
Pseudocrenilabrus multicolor	MCZ100465	10	1,5,10	X	X	X	X	X	
Pseudotropheus johannii	MCZ98611	10	2,5,8	X	X	X	X		X
Pterophyllum scalare	MCZ14989	Heroini	1,2,11	X	X	X	X	X	X
Ptychochromis oligacanthus	AMNH-I-225992	Ptychochromini	1,2,11	X	X	X	X	X	X
Pyxichromis orthostoma	MCZ153518	10		X	X	X	X		
Retroculus boulengeri	NMNH152111	Retroculini	1,2,11	X	X	X	X	X	X
Rhamphochromis macrophthalmus	MCZ49542	10	3,4,5	X	X		X		
Sargochromis codringtonii	MCZ54346	10	5	X	X	X	X		
Sarotherodon occidentalis	MCZ63196	3	1,2,7	X	X	X	X	X	X
Satanoperca jurupari	MCZ90954	Geophagini	1,2,11	X	X	X	X	X	X
Schubotzia eduardiana	MCZ135771	10		X	X	X	X		
Sciaenochromis spilostichus	MCZ49477	10	4	X	X	X	X		
Serranochromis robustus	MCZ32574	10	3,5	X	X	X	X	X	
Simochromis diagramma	MCZ50844	10	5,6,10	X	X	X	X		
Spathodus marlieri	MCZ50696	9	1,5,6,10	X	X	X	X	X	
Steatocranus gibbiceps	MCZ50479	4	1,2,9,11	X	X	X	X	X	X
Stigmatochromis woodi	MCZ49441	10		X	X	X	X		

Symphysodon discus	MCZ15834	Heroini	2,11	X	X	X	X		X
Taeniochromis holotaenia	MCZ98598	10	3	X	X	X	X		
Tangachromis dhanisi	MCZ50836	7		X	X	X	X		
Teleogramma gracile	MCZ50315	2	12	X	X	X	X		
Telmatochromis dhonti	MCZ49272	6	5,6	X	X	X	X		
Thysochromis ansorgii	MCZ48070	2	7,12	X	X	X	X		
Tilapia rendalli	MCZ98624	10	1,2,7	X	X	X	X	X	
Tramitichromis brevis	MCZ49452	10		X	X	X	X		
Trematocara unimaculatum	MCZ49262	5	6	X	X	X	X		
Trematocranus placodon	MCZ49500	10	3	X	X	X	X		
Triglachromis otostigma	MCZ49275	7	5,6	X	X	X			
Tristramella simonis	MCZ25527	3	7	X	X	X	X		
Tropheus moorii	MCZ50847	10	5,6	X	X	X	X		
Tylochromis leonensis	MCZ63194	1	1,2	X	X	X	X	X	X
Tyrannochromis macrostoma	MCZ49534	10	1,3,5	X	X	X	X	X	

References for Supplemental Table 1:

Allender, C. J., O. Seehausen, M. E. Knight, G. F. Turner, and N. Maclean. 2003. Divergent selection during speciation of Lake Malawi cichlid fishes inferred from parallel radiations in nuptial coloration. Proc. Natl. Acad. Sci. USA 100: 14074-14079.

Clabaut, C., W. Salzburger, and A. Meyer. 2005. Comparative phylogenetic analyses of the adaptive radiation of Lake Tanganyika cichlid fish: nuclear sequences are less homoplasious but also less informative than mitochondrial DNA. J. Mol. Evol. 61: 666-681.

Day, J. J., J. A. Cotton, and T. G. Barraclough. 2008. Tempo and mode of diversification of Lake Tanganyika cichlid fishes. PLoS ONE 3: e1730.

Friedman, M., B. P. Keck, A. Dornburg, R. I. Eytan, C. H. Martin, C. D. Hulsey, P. C. Wainwright, and T. J. Near. 2013. Molecular and fossil evidence place the origin of cichlid fishes long after Gondwanan rifting. Proc. R. Soc. Lond. B. 280: 20131733.

Friedman, M., B. P. Keck, A. Dornburg, R. I. Eytan, C. H. Martin, C. D. Hulsey, P. C. Wainwright, and T. J. Near. 2013. Data from: Molecular and fossil evidence place the origin of cichlid fishes long after Gondwanan rifting. Dryad Digital Repository. doi: http://dx.doi.org/10.5061/dryad.48f62.

Joyce, D. A., D. H. Lunt, M. J. Genner, G. F. Turner, R. Bills, and O. Seehausen. 2011. Repeated colonization and hybridization in Lake Malawi cichlids. Curr. Biol. 21: R108-R109.

Klett, V., and Meyer, A. 2002. What, if anything, is a tilapia? Mitochondrial ND2 phylogeny of tilapiines and the evolution of parental care systems in the African cichlid fishes. Mol. Biol. Evol. 19: 865-883.
McMahan, C. D., P. Chakrabarty, J. S. Sparks, W. L. Smith, and M. P. Davis. 2013. Temporal patterns of diversification across global cichlid biodiversity. PLoS ONE. 8: e71162.
Moran, P., I. Kornfield, and P. N. Reinthal. 1994. Molecular systematics and radiation of the haplochromine cichlids (Teleostei: Perciformes) of Lake Malawi. Copeia 1994: 274-288.
Salzburger, W., T. Mack, E. Verheyen, and A. Meyer. 2005. Out of Tanganyika: genesis, explosive speciation, key-innovations and phylogeography of the haplochromine cichlid fishes. BMC Evol. Biol. 5: 17.
Schwarzer, J., B. Misof, D. Tautz, and U. L. Schliewen. 2009. The root of East African cichlid radiations. BMC Evol. Biol. 9: 186.
Schwarzer, J., A. Lamboj, K. Langen, B. Misof, and U. K. Schliewen. 2015. Phylogeny and age of chromidotilapiine cichlids (Teleostei: Cichlidae). Hydrobiologia 748: 185-199.
Seehausen, O., E. Koetsier, M. V. Schneider, L. J. Chapman, C. A. Chapman, M. E. Knight, G. F. Turner, J. J. M. van Alphen, and R. Bills. 2003. Nuclear markers reveal unexpected genetic variation and a Congolese-Nilotic origin of the Lake Victoria cichlid species flock. Proc. R. Soc. Lond. B 270: 129-137.
Smith, W. L., P. Chakrabarty, and J. S. Sparks. 2008. Phylogeny, taxonomy, and evolution of Neotropical cichlids (Teleostei: Cichlidae: Cichlinae). Cladistics 24: 625-641.

56 Supplemental Table 2. List of geometric morphometric landmarks used to quantify body shape

Landmark	Anatomical Description/ Location
1	Anterior tip of the premaxilla
2	Dorsal tip of the premaxilla
3	Anterior-most point on the orbit
4	Anterior-most point of the supraoccipital crest
5	Posterior-most point on the orbit
6	Dorsal tip of the supraoccipital crest
7	Base of dorsal fin spine I
8	Base of middle dorsal fin spine, or, if even number of spines (N), spine N/2
9	Base of posterior-most dorsal fin spine
10	Base of dorsal fin ray 1
11	Base of middle dorsal fin ray, or if even number of spines (N), spine N/2
12	Base of posterior-most dorsal fin ray
13	Base of dorsal-most caudal fin ray
14	Center of caudal fin ray base
15	Base of ventral-most caudal fin ray
16	Base of posterior-most anal fin ray
17	Base of anterior-most anal fin spine
18	Juncture of pelvic fin bases
19	Base of the ventral-most fin ray of the pectoral fin (left)
20	Base of the dorsal-mot fin ray of the pectoral fin (left)
21	Anterior tip of the pelvic girdle
22	Ventral tip of pectoral girdle
23	Articular-quadrate joint
24	Anterior margin of the first vertebra
25	Posterior margin of the 10^{th} vertebra
26	Posterior margin of the 20^{th} vertebra
27	Distal tip of posterior-most epural.

57

58

Supplemental Table 3. Linear regression analyses of principal component scores on body (centroid) size. Bold text indicates significance at 0.05 level.

Structure	PC1	PC2
Body	β = -0.27, adj. R^2 = -0.01	**β = 1.61 , adj. R^2 = 0.07**
Caudal	β = -0.26, adj. R^2 = -0.00	β = -0.07, adj. R^2 = -0.01
Dorsal	**β = 0.71, adj. R^2 = 0.03**	β = 0.48, adj. R^2 = 0.03
Anal	β = -0.69, adj. R^2 =0.02	β = 0.03, adj. R^2 = -0.01

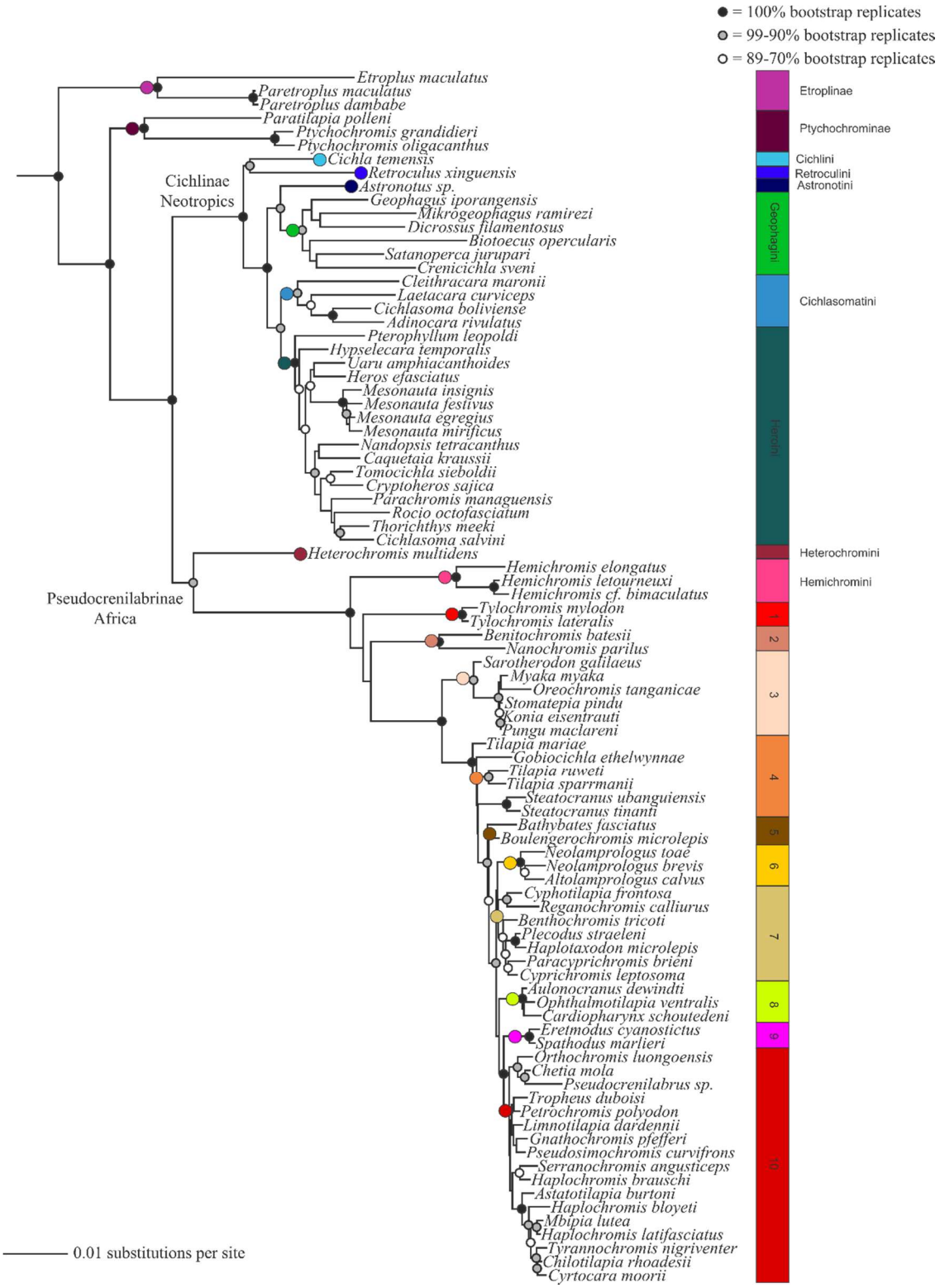

Supplemental Figure 1. Clade assignments based on Friedman *et al.* 2013. Figure reproduced and modified with permission.

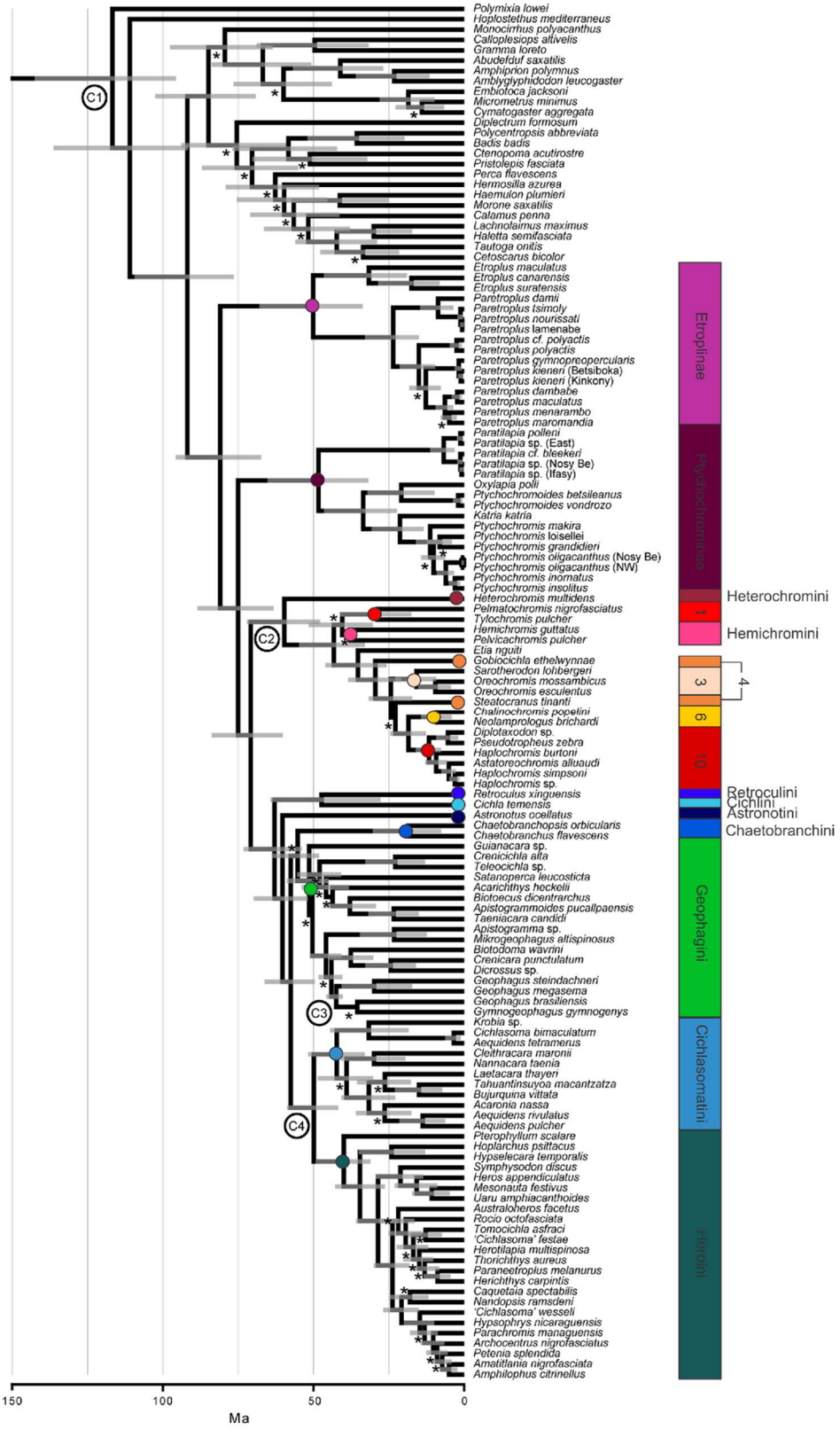

Supplemental Figure 2. Clade assignments based on McMahan et al 2013. Figure reproduced and modified with permission.

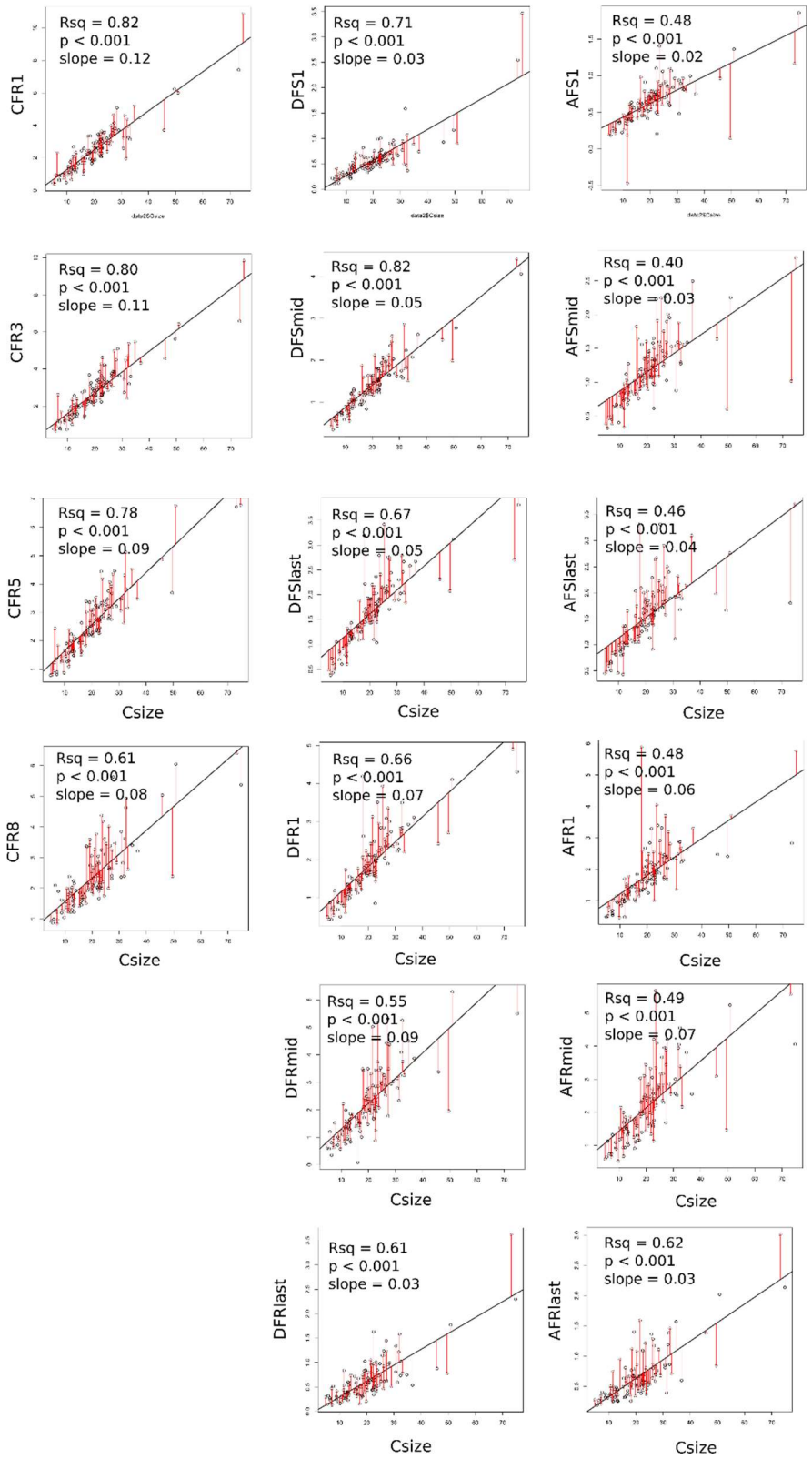

Supplemental Figure 3. Linear regressions of fin elements on body centroid size to calculate residuals which were then used in subsequent shape analyses.

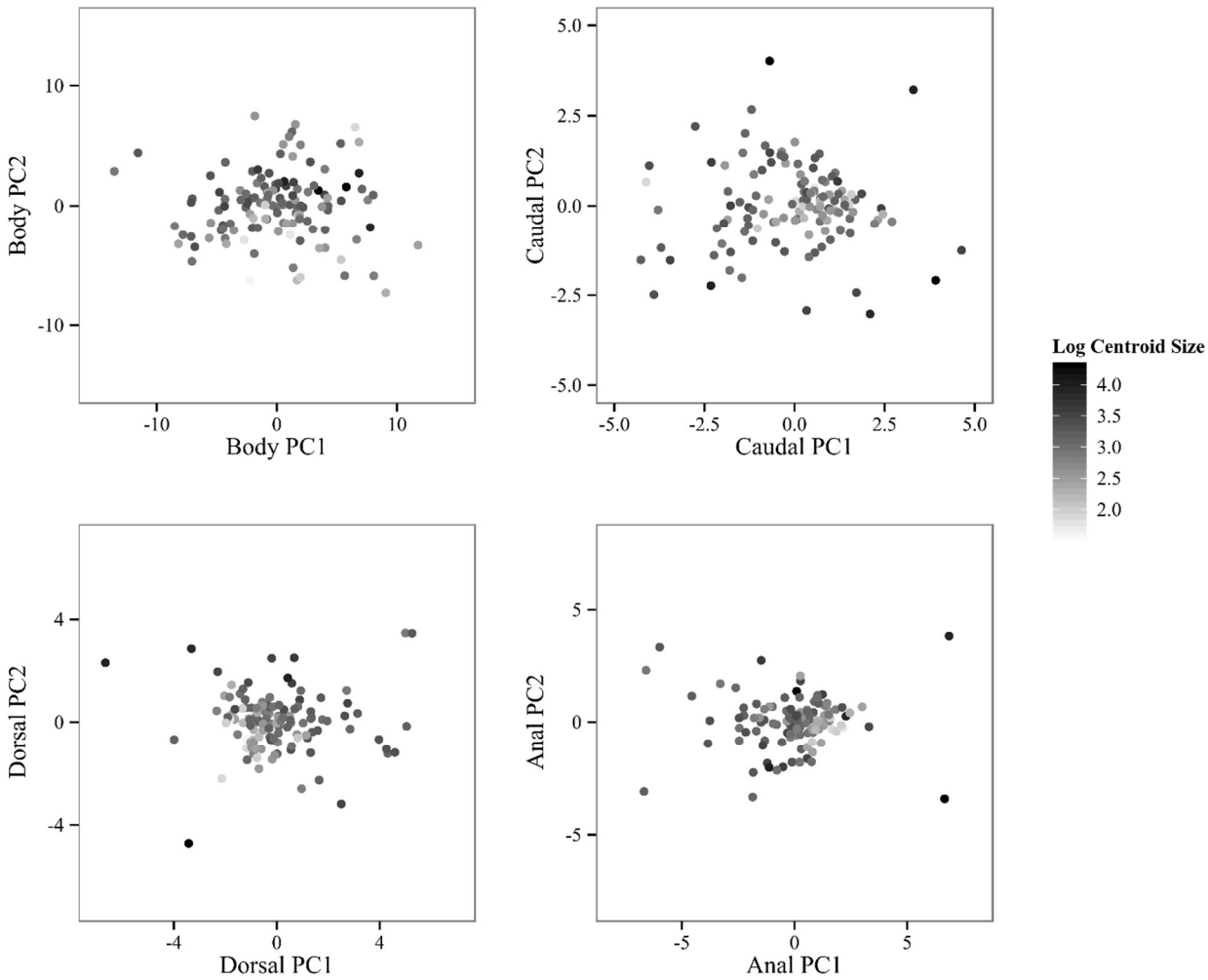

Supplemental Figure 4. Principal components of body and fin shapes colored by specimen size. From the lack of size clustering observed, it appears there are no dominant allometric patterns in body and fin shape among cichlids. Linear regressions of each PC1 and PC2 against body size revealed no allometric trends between shape and size (Supp. Table 3).

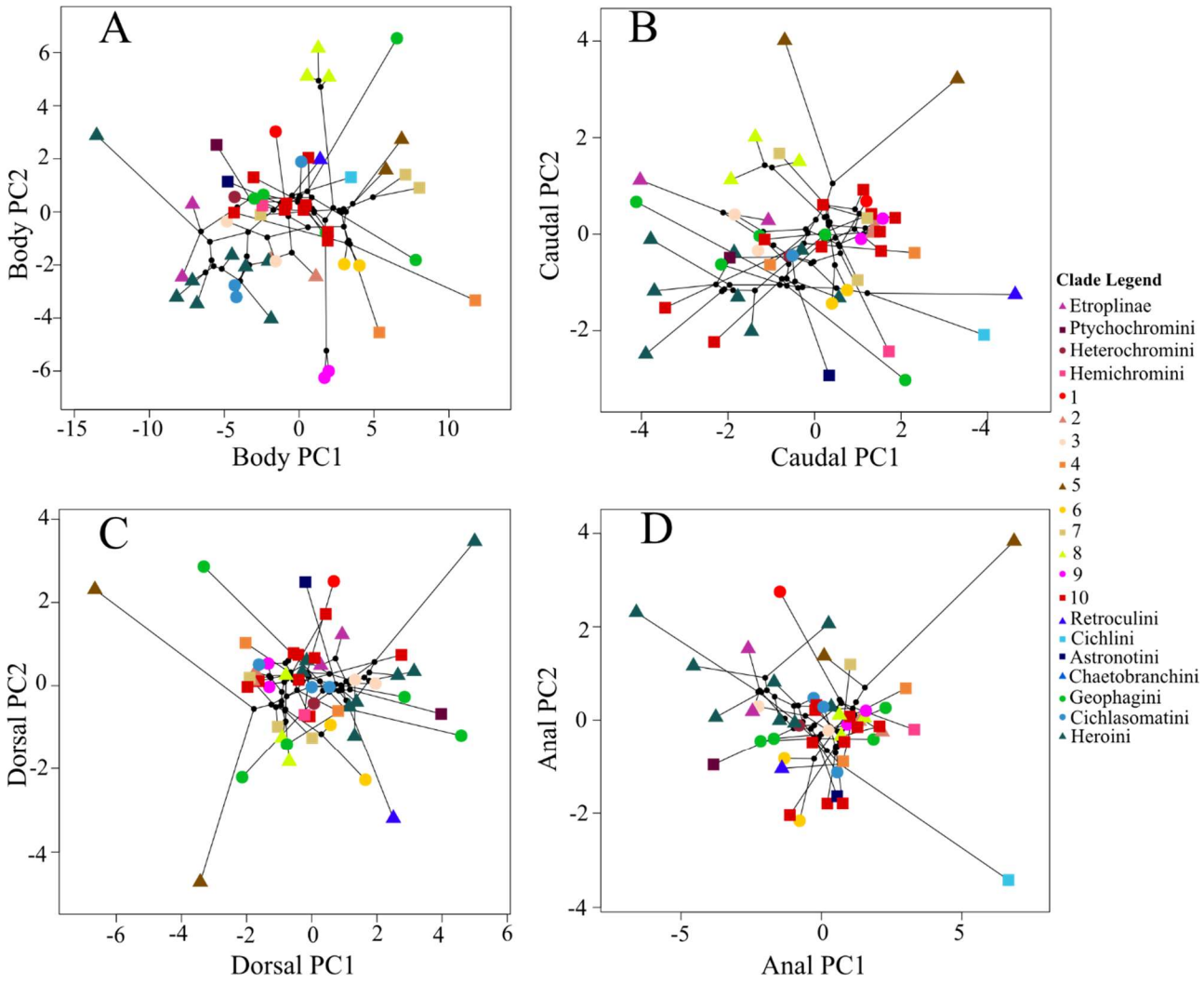

Supplemental Figure 5. Phylomorphospace of specimens represented in the Friedman et al 2013 tree, as calculated from the original PCA of all specimens.

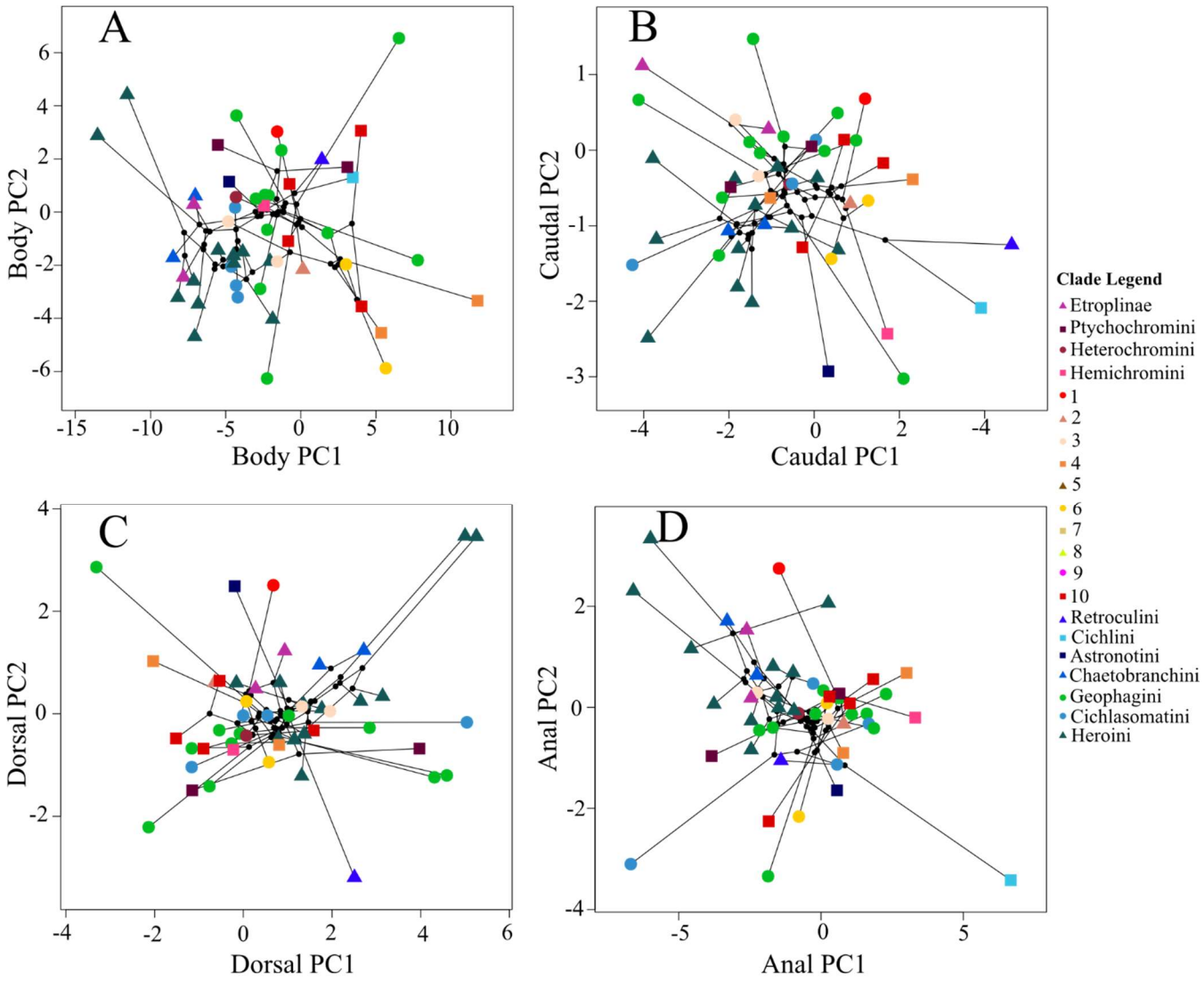

107

108 Supplemental Figure 6. Phylomorphospace of specimens represented in the McMahan et al 2013
109 tree, as calculated from the original PCA of all specimens.

110

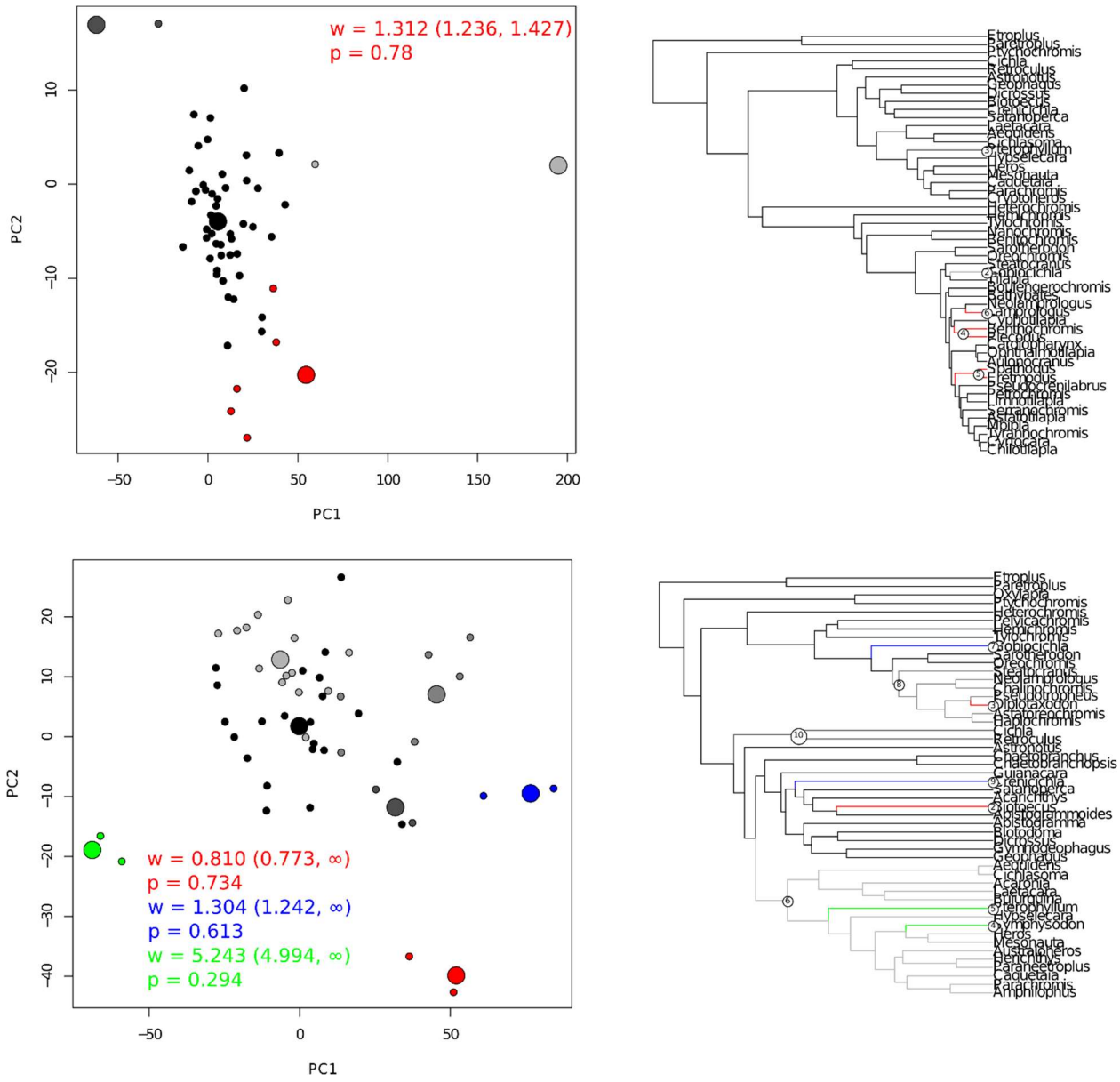

111

112 Supplemental Figure 7. SURFACE analysis and Wheatsheaf indices with 95% confidence
113 intervals for body shape on the Friedman (top) and McMahan (bottom) trees.

114

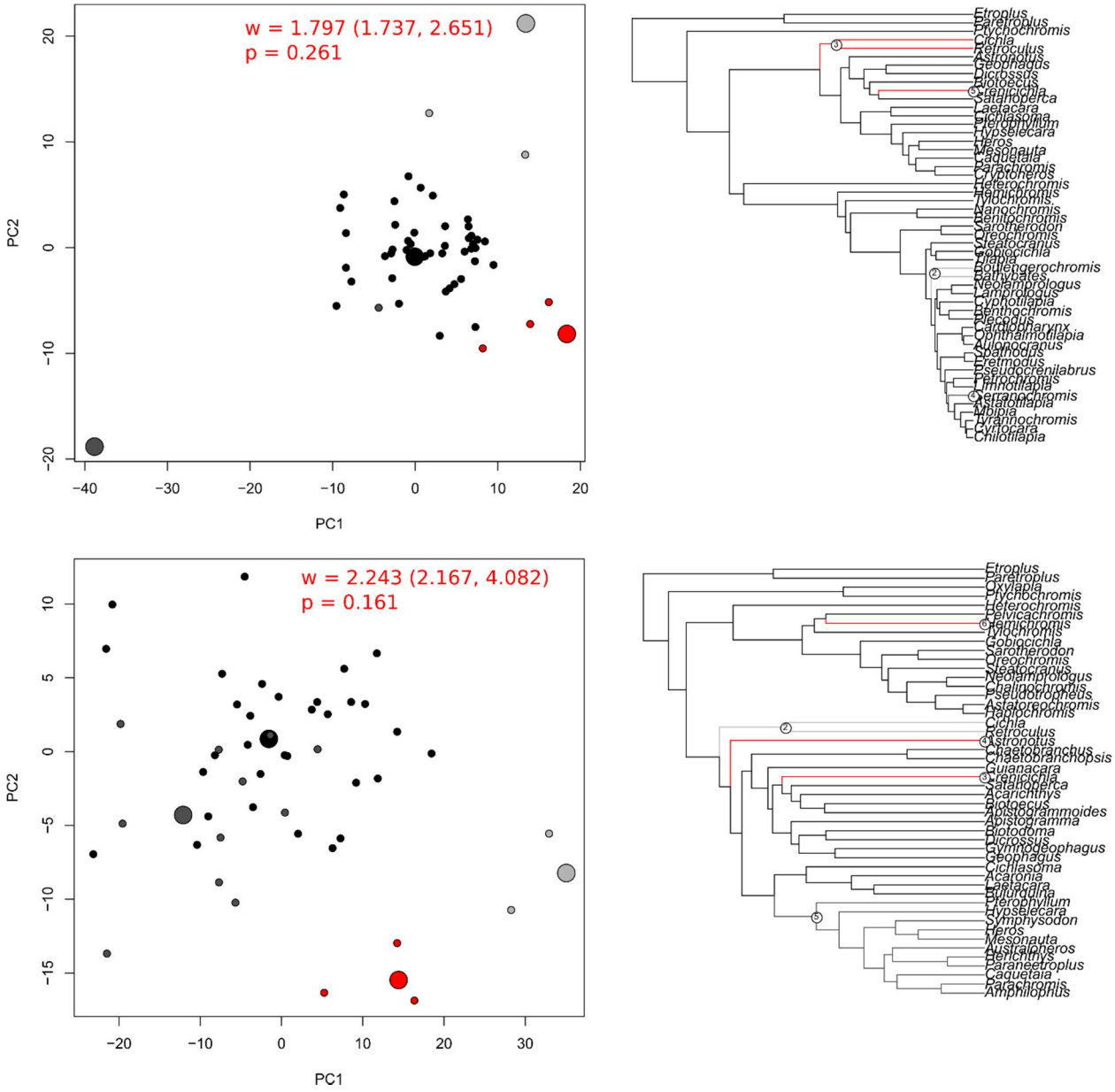

Supplemental Figure 8. SURFACE analysis and Wheatsheaf indices with 95% confidence intervals for caudal shape on the Friedman (top) and McMahan (bottom) trees.

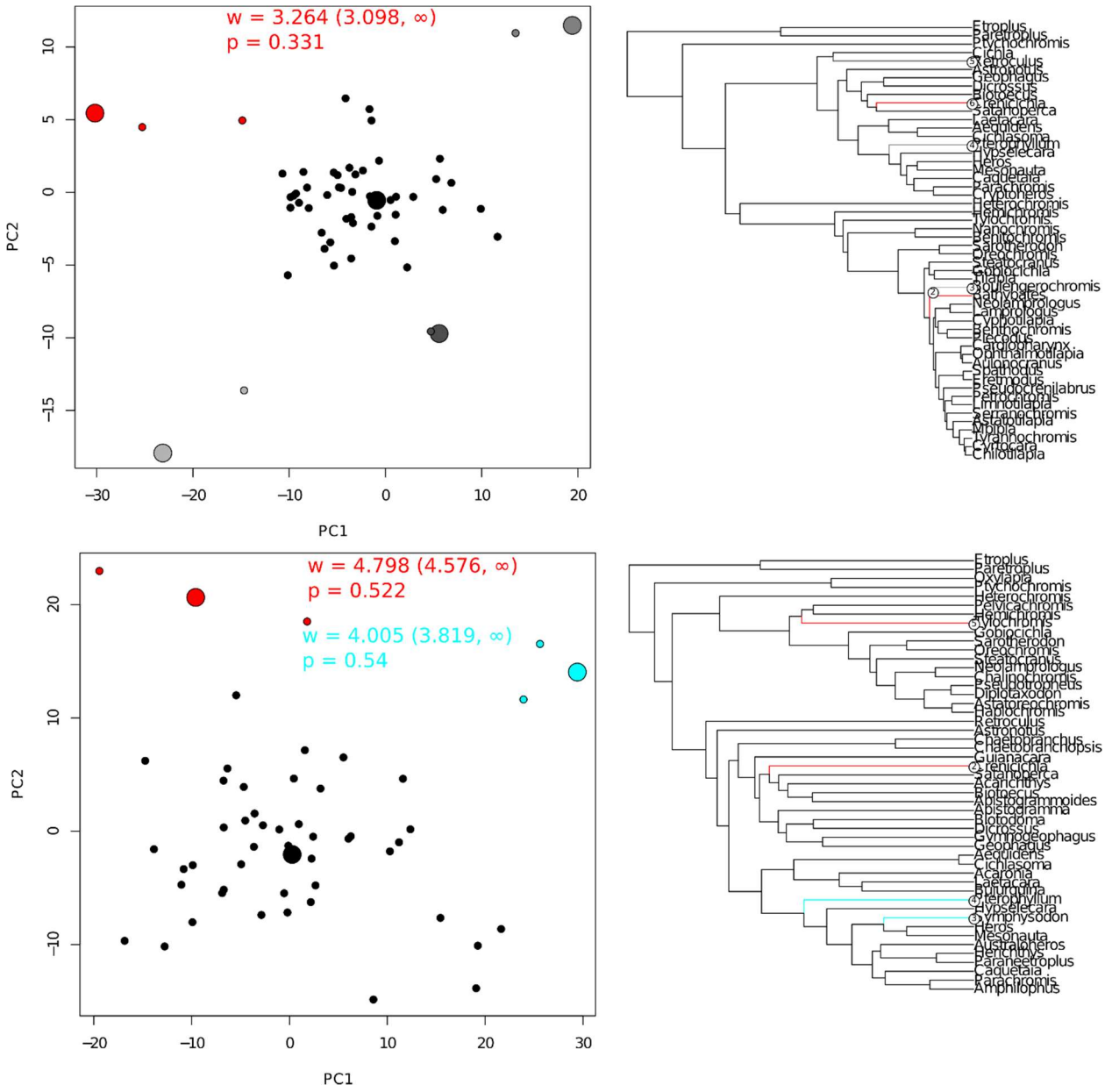

Supplemental Figure 9. SURFACE analysis and Wheatsheaf indices with 95% confidence intervals for dorsal fin shape on the Friedman (top) and McMahan (bottom) trees.

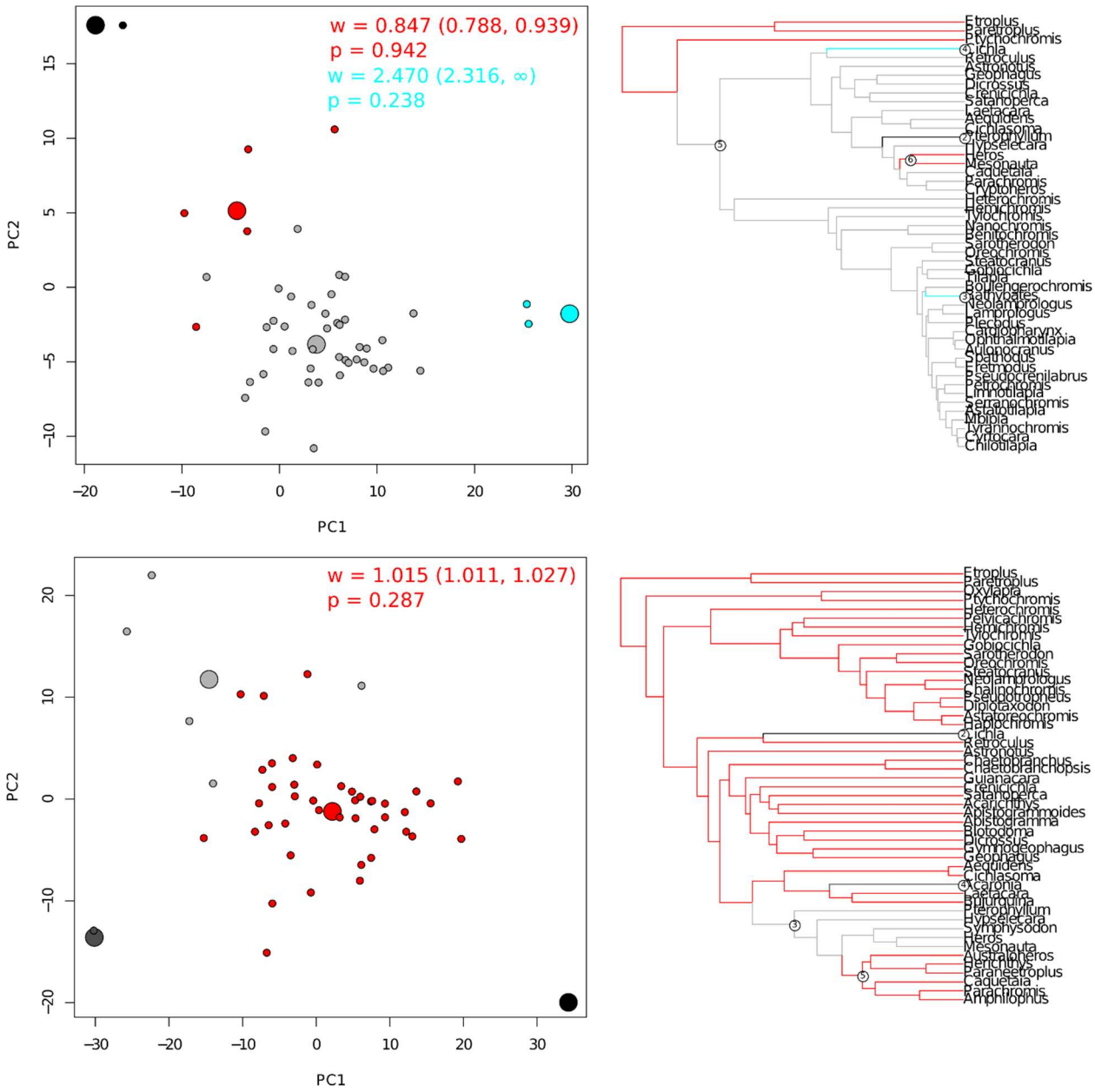

Supplemental Figure 10. SURFACE analysis and Wheatsheaf indices with 95% confidence intervals for anal fin shape on the Friedman (top) and McMahan (bottom) trees.

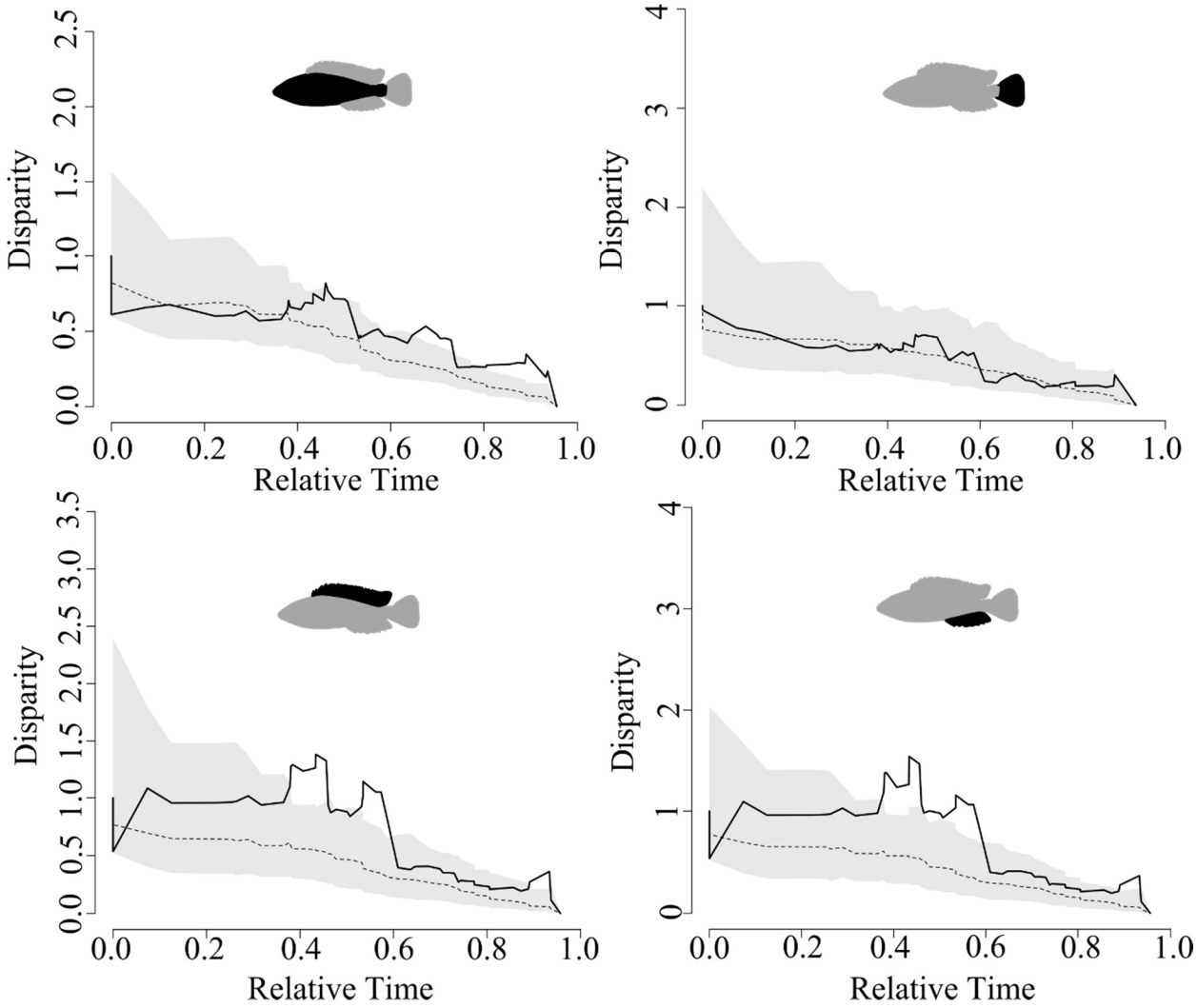

Supplemental Figure 11: Cichlid disparity through time calculated from the McMahan tree dataset (black line) with 95% confidence intervals following the method of Slater et al 2013. Mean expected disparity under the BM model is shown as the dotted line. Peaks above the grey confidence interval show higher disparity than expected under a BM model of trait evolution. Relative time is calculated from the tree length of the pruned subtrees specific to each morphological structure.

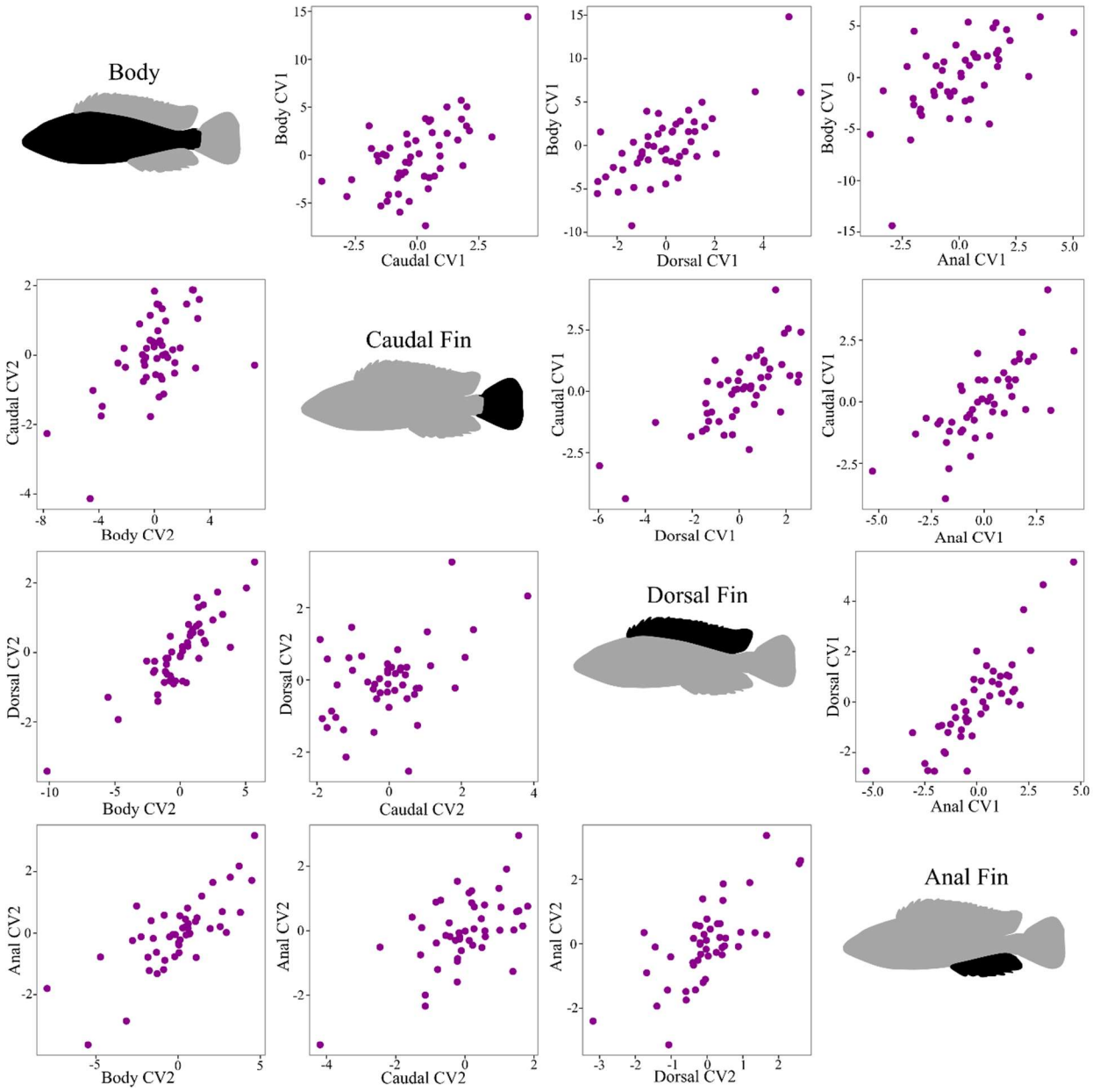

Supplemental Figure 12: Partial least squares canonical variates displaying covariation of independent contrasts of body and median fin shapes on the Friedman et al 2013 phylogeny.

Supplemental Table 4. Partial least squares canonical variate variable loadings for analyses conducted on phylogenetic independent contrasts of the Friedman tree morphological dataset. Loadings are followed by the amount of variance in each variable explained by the canonical variate (for second canonical variate pairs, this is reported as the cumulative variation explained by CV pairs 1 and 2, less the variation explained by CV pair 1). For PLS including body shape data, only the 10 body shape variables with the greatest magnitude loadings are reported. (For full statistical output, see Supp. Info.) Correlation coefficients relating each pair of partial least square canonical variates are reported in parentheses.

Body-Caudal PLS							
First CV Pair (r = 0.61)				Second CV Pair (r = 0.57)			
Variable	CV1 Body Loading	Variable	CV1 Caudal Loading	Variable	CV2 Body Loading	Variable	CV2 Caudal Loading
22y	-0.25 (89%)	CFR1	0.36(31%)	10x	-0.39 (81%)	CFR1	0.68 (60%)
18y	-0.25 (86%)	CFR3	0.51 (61%)	9x	-0.38 (80%)	CFR3	0.48 (30%)
21y	-0.24 (81%)	CFR5	0.60 (86%)	11x	-0.32 (55%)	CFR5	-0.29 (10%)
17y	-0.24 (79%)	CFR8	0.52 (65%)	13x	0.28 (42%)	CFR8	-0.49 (32%)
7y	0.24 (77%)			14x	0.28 (41%)		
19y	-0.23 (76%)			27x	0.26 (37%)		
6y	0.23 (75%)			15x	0.26 (37%)		
16y	-0.23 (73%)			5x	0.24 (32%)		
8y	0.22 (69%)			13y	-0.19 (19%)		
9y	0.21 (60%)			6x	0.18 (18%)		
Body-Dorsal PLS							
First CV Pair (r = 0.71)				Second CV Pair (r = 0.87)			
Variable	CV1 Body Loading	Variable	CV1 Dorsal Loading	Variable	CV2 Body Loading	Variable	CV2 Dorsal Loading
18y	-0.24 (87%)	Dlength	0.11 (4%)	1x	0.30 (56%)	Dlength	0.86 (80%)
22y	-0.24 (83%)	DFS1	0.03 (0%)	12x	0.29 (54%)	DFS1	-0.40 (17%)
7y	0.23 (81%)	DFSmid	0.42 (52%)	14y	-0.24 (38%)	DFSmid	-0.18 (3%)
6y	0.23 (78%)	DFSlast	0.54 (87%)	7x	-0.24 (38%)	DFSlast	0.03 (1%)
8y	0.23 (77%)	DFR1	0.52 (82%)	13y	-0.24 (36%)	DFR1	0.04 (0%)
19y	-0.23 (76%)	DFRmid	0.50 (75%)	2y	-0.22 (32%)	DFRmid	0.08 (0%)
21y	-0.23 (76%)	DFRlast	0.19 (11%)	11x	0.22 (30%)	DFRlast	-0.29 (9%)
17y	-0.23 (75%)			25y	0.21 (29%)		
16y	-0.22 (69%)			26y	0.20 (27%)		
27x	-0.21 (66%)			3x	0.20 (25%)		
Body-Anal PLS							
First CV Pair (r = 0.60)				Second CV Pair (r = 0.76)			
Variable	CV1 Body Loading	Variable	CV1 Anal Loading	Variable	CV2 Body Loading	Variable	CV2 Anal Loading
18y	0.25 (88%)	Alength	-0.17 (9%)	14y	-0.31 (59%)	Alength	0.77 (79%)
22y	0.25 (88%)	AFS1	-0.39 (48%)	13y	-0.30 (55%)	AFS1	-0.52 (36%)
21y	0.24 (79%)	AFSmid	-0.46 (69%)	27y	-0.28 (45%)	AFSmid	-0.36 (17%)
7y	-0.24 (78%)	AFSlast	-0.52 (87%)	1x	0.26 (41%)	AFSlast	0.02 (0%)
17y	0.24 (77%)	AFR1	-0.48 (74%)	25y	0.26 (40%)	AFR1	0.13 (2%)
6y	-0.24 (76%)	AFRmid	-0.37 (46%)	15y	-0.26 (39%)	AFRmid	0.15 (3%)
19y	-0.23 (76%)	AFRlast	-0.08 (2%)	10y	0.23 (33%)	AFRlast	-0.04 (0%)
8y	-0.23 (70%)			9y	0.23 (32%)		
16y	0.22 (66%)			12x	0.23 (32%)		
27x	0.21 (58%)			26y	0.22 (30%)		

Supp. Table 4, continued

Caudal-Dorsal PLS							
First CV Pair (r = 0.73)				Second CV Pair (r = 0.43)			
Variable	CV1 Caudal Loading	Variable	CV1 Dorsal Loading	Variable	CV2 Caudal Loading	Variable	CV2 Dorsal Loading
CFR1	-0.25 (14%)	Dlength	-0.08 (2%)	CFR1	-0.78 (82%)	Dlength	0.28 (8%)
CFR3	-0.44 (44%)	DFS1	0.02 (0%)	CFR3	-0.57 (43%)	DFS1	-0.88 (80%)
CFR5	-0.64 (94%)	DFSmid	-0.40 (47%)	CFR5	0.12 (2%)	DFSmid	-0.35 (13%)
CFR8	-0.60 (81%)	DFSlast	-0.53 (84%)	CFR8	0.33 (14%)	DFSlast	-0.15 (3%)
		DFR1	-0.52 (83%)			DFR1	0.01 (0%)
		DFRmid	-0.52 (80%)			DFRmid	0.24 (6%)
		DFRlast	-0.22 (15%)			DFRlast	0.17 (3%)
Caudal-Anal PLS							
First CV Pair (r = 0.72)				Second CV Pair (r = 0.58)			
Variable	CV1 Caudal Loading	Variable	CV1 Anal Loading	Variable	CV2 Caudal Loading	Variable	CV2 Anal Loading
CFR1	0.32 (25%)	Alength	0.13 (6%)	CFR1	0.71 (65%)	Alength	0.08 (1%)
CFR3	0.50 (61%)	AFS1	0.42 (57%)	CFR3	0.49 (31%)	AFS1	-0.04 (0%)
CFR5	0.61 (90%)	AFSmid	0.47 (72%)	CFR5	-0.23 (7%)	AFSmid	0.11 (1%)
CFR8	0.54 (70%)	AFSlast	0.50 (82%)	CFR8	-0.45 (27%)	AFSlast	0.31 (12%)
		AFR1	0.45 (66%)			AFR1	0.37 (17%)
		AFRmid	0.39 (49%)			AFRmid	-0.40 (20%)
		AFRlast	0.10 (4%)			AFRlast	-0.78 (75%)
Dorsal-Anal P LS							
First CV Pair (r = 0.84)				Second CV Pair (r = 0.72)			
Variable	CV1 Dorsal Loading	Variable	CV1 Anal Loading	Variable	CV2 Dorsal Loading	Variable	CV2 Anal Loading
Dlength	0.08 (2%)	Alength	0.03 (0%)	Dlength	0.54 (32%)	Alength	0.69 (75%)
DFS1	0.04 (1%)	AFS1	0.42 (55%)	DFS1	-0.73 (58%)	AFS1	-0.29 (13%)
DFSmid	0.42 (55%)	AFSmid	0.47 (70%)	DFSmid	-0.26 (7%)	AFSmid	-0.28 (12%)
DFSlast	0.52 (85%)	AFSlast	0.50 (79%)	DFSlast	-0.08 (0%)	AFSlast	-0.18 (4%)
DFR1	0.50 (77%)	AFR1	0.44 (60%)	DFR1	0.03 (0%)	AFR1	-0.21 (7%)
DFRmid	0.49 (75%)	AFRmid	0.41 (52%)	DFRmid	0.27 (8%)	AFRmid	0.42 (27%)
DFRlast	0.25 (19%)	AFRlast	0.17 (9%)	DFRlast	0.24 (6%)	AFRlast	0.36 (20%)

Supplemental Table 5. Partial least squares canonical variate variable loadings for analyses conducted on phylogenetic independent contrasts of the McMahan tree morphological dataset. Loadings are followed by the amount of variance in each variable explained by the canonical variate (for second canonical variate pairs, this is reported as the cumulative variation explained by CV pairs 1 and 2, less the variation explained by CV pair 1). For PLS including body shape data, only the 10 body shape variables with the greatest magnitude loadings are reported. (For full statistical output, see Supp. Info.) Correlation coefficients relating each pair of partial least square canonical variates are reported in parentheses.

Body-Caudal PLS							
First CV Pair (r = 0.48)				Second CV Pair (r = 0.52)			
Variable	CV1 Body Loading	Variable	CV1 Caudal Loading	Variable	CV2 Body Loading	Variable	CV2 Caudal Loading
22y	0.25 (93%)	CFR1	-0.50 (70%)	8x	-0.36 (57%)	CFR1	0.55 (28%)
18y	0.24 (88%)	CFR3	-0.57 (89%)	13y	-0.33 (49%)	CFR3	0.21 (4%)
8y	-0.24 (86%)	CFR5	-0.54 (80%)	9x	-0.32 (47%)	CFR5	-0.40 (15%)
7y	-0.23 (79%)	CFR8	-0.41 (46%)	10x	-0.32 (46%)	CFR8	-0.73 (50%)
21y	0.23 (79%)			27y	-0.30 (40%)		
9y	-0.23 (77%)			11x	-0.27 (33%)		
6y	-0.22 (76%)			12y	-0.27 (32%)		
19y	0.22 (75%)			13x	0.26 (31%)		
17y	0.22 (74%)			15x	0.24 (25%)		
10y	-0.22 (73%)			27x	0.23 (24%)		
Body-Dorsal PLS							
First CV Pair (r = 0.72)				Second CV Pair (r = 0.73)			
Variable	CV1 Body Loading	Variable	CV1 Dorsal Loading	Variable	CV2 Body Loading	Variable	CV2 Dorsal Loading
17y	-0.26 (87%)	Dlength	0.33 (33%)	12x	0.31 (59%)	Dlength	0.60 (48%)
8y	0.26 (87%)	DFS1	0.02 (0%)	11x	0.29 (52%)	DFS1	-0.33 (14%)
7y	0.26 (85%)	DFSmid	0.36 (39%)	21x	-0.26 (42%)	DFSmid	-0.21 (6%)
18y	-0.25 (83%)	DFSlast	0.54 (89%)	1x	0.26 (41%)	DFSlast	-0.02 (0%)
9y	0.24 (76%)	DFR1	0.52 (83%)	2y	-0.25 (38%)	DFR1	-0.10 (1%)
22y	-0.24 (74%)	DFRmid	0.46 (64%)	4y	-0.23 (32%)	DFRmid	-0.31 (13%)
6y	0.24 (74%)	DFRlast	-0.02 (0%)	22x	-0.21 (26%)	DFRlast	-0.69 (62%)
10y	0.24 (73%)			12y	-0.20 (25%)		
19y	-0.23 (67%)			21y	0.20 (23%)		
20y	-0.22 (58%)			16x	0.19 (22%)		
Body-Anal PLS							
First CV Pair (r = 0.66)				Second CV Pair (r = 0.61)			
Variable	CV1 Body Loading	Variable	CV1 Anal Loading	Variable	CV2 Body Loading	Variable	CV2 Anal Loading
17y	-0.27 (90%)	Alength	0.34 (40%)	26y	0.27 (48%)	Alength	0.62 (48%)
18y	-0.27 (86%)	AFS1	0.31 (33%)	23y	0.27 (46%)	AFS1	-0.53 (35%)
8y	0.26 (82%)	AFSmid	0.45 (71%)	13x	0.26 (42%)	AFSmid	-0.20 (5%)
22y	-0.26 (79%)	AFSlast	0.51 (92%	27x	0.23 (34%)	AFSlast	0.01 (0%)
9y	0.26 (79%)	AFR1	0.48 (79%)	18x	-0.22 (32%)	AFR1	-0.01 (0%)
7y	0.25 (77%)	AFRmid	0.39 (54%)	13y	-0.22 (32%)	AFRmid	-0.46 (26%)
10y	0.25 (76%)	AFRlast	0.11 (4%)	14x	0.22 (31%)	AFRlast	-0.33 (14%)
19y	-0.24 (72%)			26x	-0.21 (28%)		
20y	-0.23 (66%)			5y	-0.21 (28%)		
6y	0.23 (65%)			25x	-0.21 (27%)		

Supp Table 5, continued

Caudal-Dorsal PLS							
First CV Pair (r = 0.61)				Second CV Pair (r = 0.33)			
Variable	CV1 Caudal Loading	Variable	CV1 Dorsal Loading	Variable	CV2 Caudal Loading	Variable	CV2 Dorsal Loading
CFR1	-0.42 (50%)	Dlength	-0.09 (2%)	CFR1	0.69 (46%)	Dlength	0.21 (3%)
CFR3	-0.53 (78%)	DFS1	-0.14 (5%)	CFR3	0.41 (16%)	DFS1	0.84 (55%)
CFR5	-0.57 (91%)	DFSmid	-0.39 (38%)	CFR5	-0.20 (4%)	DFSmid	0.40 (12%)
CFR8	-0.48 (65%)	DFSlast	-0.52 (67%)	CFR8	-0.57 (31%)	DFSlast	0.20 (3%)
		DFR1	-0.57 (80%)			DFR1	0.01 (0%)
		DFRmid	-0.58 (83%)			DFRmid	-0.16 (2%)
		DFRlast	-0.21 (11%)			DFRlast	-0.36 (10%)
Caudal-Anal PLS							
First CV Pair (r = 0.67)				Second CV Pair (r = 0.52)			
Variable	CV1 Caudal Loading	Variable	CV1 Anal Loading	Variable	CV2 Caudal Loading	Variable	CV2 Anal Loading
CFR1	0.42 (48%)	Alength	0.18 (12%)	CFR1	0.70 (45%)	Alength	0.37 (17%)
CFR3	0.53(78%)	AFS1	0.38 (53%)	CFR3	0.44 (18%)	AFS1	-0.06 (0%)
CFR5	0.57 (91%)	AFSmid	0.45 (72%)	CFR5	-0.23 (5%)	AFSmid	0.23 (7%)
CFR8	0.48 (65%)	AFSlast	0.48 (82%)	CFR8	-0.58 (31%)	AFSlast	0.30 (12%)
		AFR1	0.44 (72%)			AFR1	0.28 (10%)
		AFRmid	0.45 (73%)			AFRmid	-0.35 (15%)
		AFRlast	0.17 (10%)			AFRlast	-0.75 (72%)
Dorsal-Anal P LS							
First CV Pair (r = 0.88)				Second CV Pair (r = 0.70)			
Variable	CV1 Dorsal Loading	Variable	CV1 Anal Loading	Variable	CV2 Dorsal Loading	Variable	CV2 Anal Loading
Dlength	0.28 (23%)	Alength	0.24 (22%)	Dlength	-0.49 (32%)	Alength	0.16 (3%)
DFS1	0.06 (1%)	AFS1	0.34 (46%)	DFS1	0.33 (15%)	AFS1	-0.14 (2%)
DFSmid	0.40 (48%)	AFSmid	0.44 (74%)	DFSmid	0.02 (0%)	AFSmid	-0.29 (9%)
DFSlast	0.53 (86%)	AFSlast	0.46 (83%)	DFSlast	-0.13 (2%)	AFSlast	-0.27 (7%)
DFR1	0.51 (79%)	AFR1	0.43 (71%)	DFR1	0.01 (0%)	AFR1	-0.14 (2%)
DFRmid	0.48 (69%)	AFRmid	0.44 (73%)	DFRmid	0.32 (14%)	AFRmid	0.36 (13%)
DFRlast	0.04 (0%)	AFRlast	0.22 (18%)	DFRlast	0.78 (82%)	AFRlast	0.84 (73%)